JOURNAL OF GEOPHYSICAL RESEARCH, VOL. 101, NO. E7, PAGES 16,841–16,843, JULY 25, 1996

The lunar crust: Global structure and signature of major basins

Gregory A. Neumann and Maria T. Zuber[1]

Department of Earth and Planetary Sciences, Johns Hopkins University, Baltimore, Maryland

David E. Smith and Frank G. Lemoine

Laboratory for Terrestrial Physics, NASA/Goddard Space Flight Center, Greenbelt, Maryland

Abstract. New lunar gravity and topography data from the Clementine Mission provide a global Bouguer anomaly map corrected for the gravitational attraction of mare fill in mascon basins. Most of the gravity signal remaining after corrections for the attraction of topography and mare fill can be attributed to variations in depth to the lunar Moho and therefore crustal thickness. The large range of global crustal thickness (~20-120 km) is indicative of major spatial variations in melting of the lunar exterior and/or significant impact-related redistribution. The 61-km average crustal thickness, constrained by a depth-to-Moho measured during the Apollo 12 and 14 missions, is preferentially distributed toward the farside, accounting for much of the offset in center-of-figure from the center-of-mass. While the average farside thickness is 12 km greater than the nearside, the distribution is nonuniform, with dramatic thinning beneath the farside, South Pole-Aitken basin. With the global crustal thickness map as a constraint, regional inversions of gravity and topography resolve the crustal structure of major mascon basins to half wavelengths of 150 km. In order to yield crustal thickness maps with the maximum horizontal resolution permitted by the data, the downward continuation of the Bouguer gravity is stabilized by a three-dimensional, minimum-slope and curvature algorithm. Both mare and non-mare basins are characterized by a central upwarped moho that is surrounded by rings of thickened crust lying mainly within the basin rims. The inferred relief at this density interface suggests a deep structural component to the surficial features of multiring lunar impact basins. For large (>300 km diameter) basins, moho relief appears uncorrelated with diameter, but is negatively correlated with basin age. In several cases, it appears that the multiring structures were out of isostatic equilibrium prior to mare emplacement, suggesting that the lithosphere was strong enough to maintain their state of stress to the present.

Introduction

Large, uncompensated density anomalies ("mascons") coincide with most nearside lunar mare basins [*Muller and Sjogren*, 1968]. These anomalies arise in part from the effects of impact processes on crustal structure [e.g., *Wise and Yates*, 1970; *Bowin et al.*, 1975; *Phillips and Dvorak*, 1981; *Bratt et al.*, 1985a,b] and in part from subsequent volcanic flooding by denser mare basalt [*Conel et al.*, 1968; *Phillips et al.*, 1972; *Solomon and Head*, 1980]. Previous analyses [*Sjogren and Smith*, 1976; *Bills and Ferrari*, 1977b; *Thurber and Solomon*, 1978; *Bratt et al.*, 1985a] have attempted to constrain the crustal structure in association with the major basins in spite of limited topographic coverage and uncertainties in the gravity field. Such deficiencies have so far prevented a uniform and comprehensive analysis of lunar basin structure. *Phillips and Dvorak* [1981] used topography from Earth-based radar, characterized by vertical errors of up to 500 m, to model gravity derived from line-of-sight tracking over the Grimaldi basin. *Bratt et al.* [1985a] used topographic data from a variety of sources, and gravity calculated from a multidisk mass model [*Wong et al.*, 1971, 1975] to invert for the depth of the lunar moho in 5x5 degree blocks. They assumed that the premare basins had achieved nearly complete isostatic balance through viscous relaxation [*Solomon et al.*, 1982] prior to being filled with mare basalts. The 2- to 4.5-km thicknesses of mare basalts inferred by Bratt et al. were insufficient to produce the measured positive gravity anomaly over the mare basins. They concluded that the mare basins were characterized by significant central uplift of mantle following impact.

Geophysical data from the Clementine mission and reanalysis of historical tracking have now shown that the lunar lithosphere had a variable mechanical structure and was, on average, more rigid during the period of basin formation than previously thought [*Zuber et al.*, 1994]. These data permit a consistent analysis and comparison of crustal structure of lunar basins, without isostatic assumptions. We apply a complete Bouguer correction to the lunar gravity field of F.G. Lemoine et al. (GLGM2: A 70th degree and order lunar gravity model from Clementine and historical data, submitted to *Journal of Geophysical Research*, 1995; hereinaftrer referred to as submitted manuscript), using the Clementine topography (D. E. Smith et al., The topography of the Moon

[1]Now at Department of Earth, Atmospheric and Planetary Sciences, Massachusetts Institute of Technology, Cambridge.

Paper number 96JE01246.
0148-0227/96/96JE-01246$09.00

from the Clementine LIDAR, submitted to *Journal of Geophysical Research*, 1996; hereinafter referred to as submitted manuscript). The resulting Bouguer anomalies are modeled by topography on the lunar Moho, assuming a constant-density crust and mantle. The difference between the inferred moho topography and the surface topography we shall refer to as the crustal thickness.

A preliminary Clementine global crustal thickness map [*Zuber et al.*, 1994], in spherical harmonic degrees up to 30 (half wavelength resolution of 180 km), also showed substantial crustal thinning beneath the major basins. The Bouguer anomaly was mapped to a single mass sheet at moho depth. Finite amplitude effects were not considered, nor were loads due to the greater density of mare basalts. In this study we apply a further correction for up to 10 km of mare lavas that may have filled major basins subsequent to impact [*DeHon*, 1979]. Thicknesses of surface flows are inferred primarily from photogeologic mapping [*DeHon and Waskom*, 1976; *Horz*, 1978; *Solomon and Head*, 1980; *Head*, 1982]. Regional inversions using a quasi-continuous, minimum-structure inversion technique resolve subsurface structure of major basins at the highest resolution permitted by the gravity and topography data.

Crustal thickness and density variations play a major role in the structure of lunar basins [*Wise and Yates*, 1970; *Scott*, 1974; *Bowin et al.*, 1975; *Bills and Ferrari*, 1977b; *Phillips and Dvorak*, 1981; *Bratt et al.*, 1985a]. The largest impact basins on the Moon, as well as other terrestrial planets, are surrounded by multiple, concentric mountain rings [*Hartmann and Kuiper*, 1962]. The origin of these rings has been ascribed to the surficial effects of the impact, structural modification of the initial crater, or in strength variations of the lunar surface [e.g., *Van Dorn*, 1968; *Baldwin*, 1972; *Dence*, 1973; *Melosh*, 1982; *Spudis*, 1993]. These macroscopic features have been studied mainly by means of surface images. We now probe the lunar interior to elucidate the density structure of impact basins.

Altimetry

The LIDAR instrument aboard the polar-orbiting Clementine spacecraft [*Nozette et al.*, 1994] ranged to most of the lunar surface from 78°S to 78°N, covering the known or hypothesized major basin structures tabulated by *Wilhelms* [1987] and confirming several probable basins [*Spudis et al.*, 1994]. Clementine measured a 16-km range of topography, 30% greater than previously mapped, with the deepest and highest topography on the farside South Pole-Aitken (SP-Aitken) basin and its northern rim [*Zuber et al.*, 1994]. Such large farside excursions were detected by the Soviet Zond 3 spacecraft measurements, but could not be confirmed (B.G. Bills, personal communication, 1995). The calibration and processing of the LIDAR data from Clementine are described by D.E. Smith et al. (submitted manuscript, 1996). While the altimetry along-track is fairly dense, the east-west coverage is limited by the 2.8° spacing of the ground tracks, repeating every 132 revolutions. Polar latitudes and cross-track regions were filled in by minimum-curvature interpolation [*Smith and Wessel*, 1990] to produce the gridded Goddard Lunar Topographic Model 2 (GLTM2) (D. E. Smith et al., submitted manuscript, 1996). A spherical harmonic model complete to degree and order 70 was generated by numerical integration over the associated Legendre polynomials, without placing constraints on the power spectrum.

Uncertainty in the range data results from the behavior of the electronic subsystems under varying conditions, particularly the roughness of the surface. The detection system incorporated a programmable range window that selected only those returns near the estimated range to lunar surface, but in some cases there were many false returns within a range window. Returns from the highland regions were particularly hard to discriminate from noise due to greater dispersion of incident pulses by rough terrain. As a result, there are areas of poor data quality as well as gaps due to operational problems. Nevertheless, the accuracy of the topography is better than 100 m at the level of resolution of the spherical harmonic model.

Astronomical occultations [*Watts*, 1963; *Morrison and Martin*, 1971] provide some data near the limbs, but are not geodetically referenced. Few of the major basins were adequately sampled by the near-equatorial ground tracks of the laser altimeters aboard three Apollo Orbiters. These ground tracks lie within 26°N to 26°S latitude, and are very sparse compared with the Clementine data set. The RMS residual between the Apollo dataset and GLTM2 is more than a kilometer (D. E. Smith et al., submitted manuscript, 1996), with most of the uncertainties in topographic knowledge on the farside. Many differences in altimetry are due to undersampling. The variance of highland topography is as much as 1.25 km (1 standard deviation) over a distance of 80 km, the approximate track-to-track spacing of the Clementine orbits, compared to approximately 100 m variance over the mare. Lemoine et al. (submitted manuscript, 1995) inferred errors of up to several kilometers in the orbits used to reduce the Apollo data. Interpreting the Apollo topography [*Kaula et al.*, 1972, 1973, 1974; *Davies et al.*, 1987] required caution. The error in the present data set is nearly an order of magnitude less.

The historical data resulted in a topographic field to spherical harmonic degree and order 12 [*Bills and Ferrari*, 1977a], revealing an offset of 2 km of the center-of-figure from the center-of-mass toward the lunar farside. A long-wavelength analysis of crustal structure suggested a global dichotomy [*Kaula et al.*, 1972] arising either from different degrees of melting on the nearside and farside [*Kaula et al.*, 1972], asymmetrical bombardment [*Wood*, 1973], or large-scale internal convection [*Lingenfelter and Schubert*, 1973].

Gravity

Uncertainty in the lunar gravity field limits resolution of the interior density structure. The 70th degree and order Goddard lunar gravitational model GLGM2 (F. G. Lemoine et al., submitted manuscript, 1995), a calibrated solution based on Clementine and Apollo tracking data, succeeded a preliminary model GLGM1 [*Zuber et al.*, 1994]. The most recent pre-Clementine gravity model [*Konopliv et al.*, 1993] had unreasonably large short-wavelength power (a range of 1000 mGal) when evaluated at the surface. The power spectrum of GLGM2, originally designated lgm0309a, is damped by an a priori "Kaula's rule" [*Kaula*, 1966] constraint that acts as a low-pass filter to supress artifacts where unconstrained by low-altitude tracking. Such a constraint has the drawback that some of the power in the tracking data over the nearside basins is not modeled. We use a companion model, lgm0309b (F. G. Lemoine et al., submitted manuscript, 1995), that is identical to GLGM2 but with a weaker spectral constraint. The total range of GLGM2, 652 mGal, and lgm0309b, 700 mGal, is

considerably larger than the 450 mGal of the previous degree 16 model of *Bills and Ferrari* [1980].

Figure 1 shows the coefficient variance of lgm0309b, together with the magnitude of its formal uncertainty. Beyond degree 40 the signal power declines below Kaula's rule (dashed curve), and the uncertainty becomes dominant. Formal uncertainties, when mapped to the surface, range from 14 mGal standard deviation over the equatorial nearside, to 44 mGal over the high-latitude regions of the farside.

Matching Lunar Gravity and Topography

Gravity anomalies result from the effects of surface and subsurface density contrasts. A Bouguer correction models and removes the anomaly due to surface topography. The remaining gravity signal arises from subsurface density variations. The anomalous potential at radius R_0 resulting from radial perturbations C_{lm} of an interface at radius R for degree l and order m is

$$U_{lm}=C_{lm}\frac{3\Delta\rho}{\bar{\rho}(2l+1)}\xi^{l}, \quad (1)$$

where $\Delta\rho$ is the density contrast at the interface, $\bar{\rho}$ is the mean lunar density, and $\xi=R/R_0$ is the dimensionless radius. In the case where $\Delta\rho$ is the density of the crust and $\xi=1$, U_{lm} is the Bouguer correction to the potential.

Our lunar gravity fields are derived from line-of-sight Doppler residuals of satellites tracked at minimum elevations of 40 km. Upward decay of U_{lm} at high degrees means that much of the signal that should result from topography is not resolved in the spherical harmonic solution. Figure 1 shows that the signal predicted by either an uncompensated or an Airy-compensated lunar crust (shaded region) exceeds the observed short-wavelength anomaly and is largely incoherent with it. Models using such a Bouguer correction (the uncompensated case) would tend to overestimate crustal thickness variations. To avoid bias, the same method should be employed to calculate the magnitude of the Bouguer correction as used to infer the free-air gravity. This has not been practical, given the roughly 709,000 tracking observations and 5000 model parameters incorporated in GLGM2. To obtain an unbiased, albeit noisy, Bouguer anomaly, we filter the topographic correction as if it were observed at an elevation of 32 km (Figure 1). The resulting correction nearly matches the strength of the gravity field at intermediate degrees (10 to 30) where the signal-to-noise ratio is good. This filter mainly attenuates power at higher degrees where the signal is small and where the noise level is comparatively large.

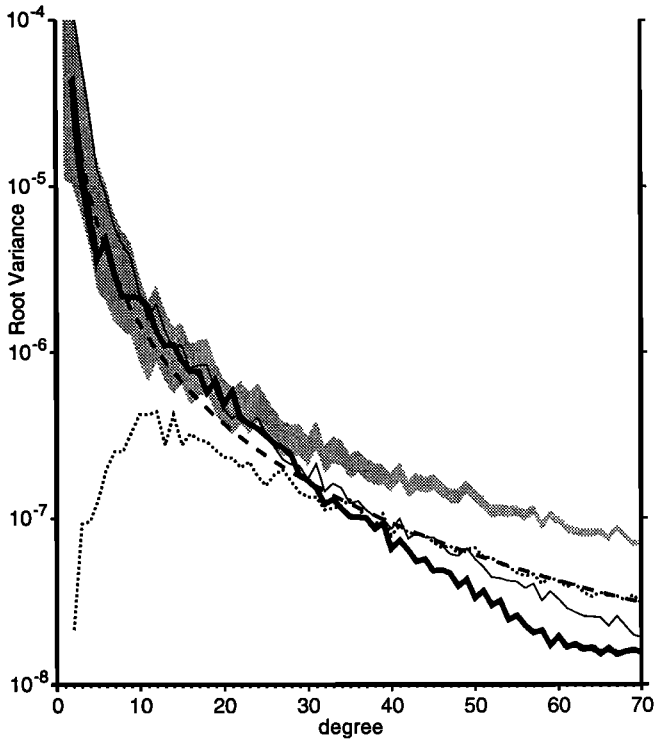

Figure 1. Coefficient variance of lunar gravity model lgm0309b (solid curve); formal noise estimate (dashed curve); and variance predicted by Bouguer and Airy-compensated models of topography (shaded region). Neither model matches the gravity spectrum, but a 32-km, upward continuation filter applied to the Bouguer correction provides an approximate match to degree 40.

The densities of nonmare lunar samples [e.g., *Talwani et al.*, 1973; *Solomon*, 1975, 1978] range from 2800 to 3000 kg m^{-3}. We choose the lesser value for $\Delta\rho$ so as to allow for the lower bulk densities of brecciated material. The lower density also avoids overcorrections that might exaggerate subsurface variation. *Solomon* [1978] utilized Apollo altimetry and geochemical data to show that density correlates with, and may partially compensate, topography via Pratt isostasy. Such regional variations may help explain the elevation of the lunar highlands, but play a lesser role at the impact basin scale, where impact-related brecciation and comminution could be more significant. Even at the scale of the highlands, however, Pratt isostasy is incapable of explaining the magnitude of gravity anomalies, and so at least some fraction of compensation must be accommodated by an Airy mechanism. Crustal density might be estimated regionally by correlating gravity with topography [*Wieczorek and Phillips*, 1996]. However, such an approach applied to lunar highland crust appears to be characterized by spectral leakage from mare regions. In our approach we assume a constant density for nonmare crust.

Central mascon maria may be filled with up to 10 km of basalt flows [*Solomon and Head*, 1980], whose density is greater than that of the surrounding crust. The gravitational attraction of the additional mass due to the difference in density is incorporated into the complete Bouguer correction, assuming a mare density of 3300 kg m^{-3}. Irregular maria such as Tranquillitatis, Nubium, and Oceanus Procellarum are estimated to have less than 1.5 km fill and average between 200 and 400 m [*DeHon*, 1974, 1977, 1978, 1979; *DeHon and Waskom*, 1976]. We shall only correct for the central mascon maria, the others having negligible effect on our results. These mare thicknesses may be overestimated, as argued by *Williams and Zuber* [1996], in which case the mascon anomalies will generally be greater.

Matching Global and Regional Downward Continuation to Crustal Thickness Constraints

We adopt two approaches to the calculation of Bouguer anomalies and crustal thickness. The only direct measurement of crustal thickness lies midway between the Apollo 12 and 14 landing sites, approximately 55 km at 3°S, 340°E [*Nakamura et al.*, 1979; *Goins et al.*, 1981]. Downward continuation of the Bouguer anomaly using equation (1) should produce a

crustal thickness map matching this constraint. The global approach, as utilized in *Zuber et al.* [1994], obtained a spherical harmonic representation to degree 30 of the Bouguer anomaly by applying a simple topographic correction to the gravity field. The resulting anomalous potential was downward continued to an equivalent mass sheet at a depth of 64 km. This mass sheet was interpreted as variations in moho topography, whereby crust is replaced by denser mantle rock.

The crustal thicknesses reported by *Zuber et al.* [1994] approached zero beneath the central portions of Mare Orientale and Mare Crisium, and parts of SP-Aitken. These thicknesses are anomalously low due to the simplified assumptions involved in their approach, and are not consistent with the apparent lack of mantle ejecta from Orientale [*Belton et al.*, 1994]. The added mass of the surficial mare basalts provides a significant correction. We represented the thicknesses of the mare basalts for eight major basins, given by *Solomon and Head* [1980], as spherical harmonics and incorporated their anomalous masses into the Bouguer corrections.

Downward continuation of the Bouguer anomaly is unstable in the presence of noise. To produce a global crustal thickness map (Plate 1), high degree spherical harmonics are filtered using an optimal method described below. This method gives a conservative estimate of crustal thickness variations, so that the moho topography nowhere reaches the lunar surface. The large amplitude of the resulting moho topography warrants a nonlinear, three-dimensional (3-D) treatment. To obtain higher-resolution maps of nearside basins where the gravity is relatively accurate, we use a finite-amplitude regional approach, wherein the regionally averaged depth to moho from the global solution constrains the average depth of the moho in each regional solution.

Surface Topography

Topographic corrections may easily be performed on regional data sets using the gravity forward-modeling algorithm of *Parker* [1972]. This algorithm fully accounts for the 3-D, large-amplitude nature of topography. The Fourier transform of the gravity anomaly at wavenumber $\mathbf{k}$, $\hat{g}(\mathbf{k})$, due to a density increase $\Delta\rho$ across the surface $h(x)$ measured at a reference depth a can be expressed as the series

$$\hat{g}(\mathbf{k}) = 2\pi\Delta\rho G e^{-a|\mathbf{k}|}\sum_{n=1}^{\infty}\frac{|\mathbf{k}|^{n-1}}{n!}\hat{F}\left[h^n\right](\mathbf{k}) \tag{2}$$

in terms of the Fourier transform $\hat{F}$ of powers of topography. Rapid and stable calculation of the Bouguer correction to within 1 mGal results from the fast Fourier transform (FFT) applied to the first four terms of the expansion. The Bouguer anomaly is the free air anomaly (FAA) minus the correction to the equation (1) potentials.

The Parker expansion (2) requires a projection of the lunar surface and moho topography onto a plane in the region of interest. Such an approximation is reasonable for calculations involving topography of a few percent of the lunar radius R_0, and results in less than 5% model error even for the largest basins. We apply an oblique Mercator projection from local polar coordinates to local Cartesian coordinates, centered on the peak gravity anomaly of each mare basin. The resulting square map regions are roughly 2048 km on a side, with a grid spacing of 8 km. This projection results in distortion increasing to a maximum of 8% at the corners of the square. Negligible distortion occurs within most basins. In order to minimize edge effects, the projected data are mirrored about both the x and y axes prior to the FFT.

Mare Loads

The Parker algorithm may also be used to correct for the additional gravitational effects due to the replacement of part of the crust by denser mare basalts. Following *Solomon and Head* [1980], we approximate the mare as one or more concentric cylindrical bodies starting at the depth of the mare floor. Since we have already performed a surface Bouguer correction, we use a density contrast of 500 kg m^{-3}, rather than the full mare density. The corrected Bouguer anomaly (CBA), the Bouguer anomaly minus the gravity due to the attraction of mare fill, reflects density variations below the near surface.

In order to make the stacked mare cylinders correspond closely to the centers of the mascons, particularly for Mare Imbrium, we adjusted the centers of the mare, where noted in Table 1, from the basin coordinates inferred from surficial features by *Wilhelms* [1987]. The basin locations are better constrained by the new topographic data. The adjustments and their consequences for gravity are, in any case, minor relative to the resolution of the gravity fields.

Prescription for Downward Continuation

Because gravity interpretation is necessarily nonunique, we model the gravity anomaly exclusively in terms of the topographic effects of density contrasts at the surface and at the lunar moho. Of all moho models, we seek the simplest that is required to fit the Bouguer gravity anomaly within its confidence limits. This entails joint minimization of some measure of model complexity as well as data misfit. The norm of solution length is one such measure [*Franklin*, 1970], but the resulting models may tend toward Kronecker delta functions. *Constable et al.* [1987] argue that the simplest model is that which is maximally flat, that is, the norms of the model slope and/or curvature should be minimized. These latter norms suppress the short-wavelength excursions of the model in proportion to the wavenumber or the wavenumber squared, respectively. An analog in the frequency domain [*Müller and Smith*, 1993; *Phipps Morgan and Blackman*, 1993] exploits the computational efficiency and stability of the FFT algorithm.

We seek the amount of topography on a hypothetical moho interface required to match a given gravity signal. Because the mass anomaly is distributed over a sheet of finite thickness, the gravity response to topography is nonlinear. Following *Oldenburg* [1974] and *Parker and Huestis* [1974], the expansion (2) can be rearranged to yield an iterative solution for $h(x)$:

$$\hat{h}(\mathbf{k}) = \frac{w(\mathbf{k})\hat{g}e^{a|\mathbf{k}|}}{2\pi\Delta\rho G} - \sum_{n=2}^{\infty}\frac{|\mathbf{k}|^{n-1}}{n!}\hat{F}\left[h^n\right](\mathbf{k}) \tag{3}$$

The first term in equation (2) is the Fourier coefficient of the topography corresponding to the simple downward continuation to a mass sheet at the moho. The factor e^{ak}, where $k = |\mathbf{k}|$, diverges rapidly for large wavenumbers, so that short wavelengths must be smoothed or truncated for stable downward continuation. We apply the filter of *Phipps Morgan and Blackman* [1993]:

$$w(\mathbf{k}) = \frac{\left(2\pi G e^{-ak}\right)^2}{\Lambda_1 k^2 + \Lambda_2 k^4 + \left(2\pi G e^{-ak}\right)^2} \tag{4}$$

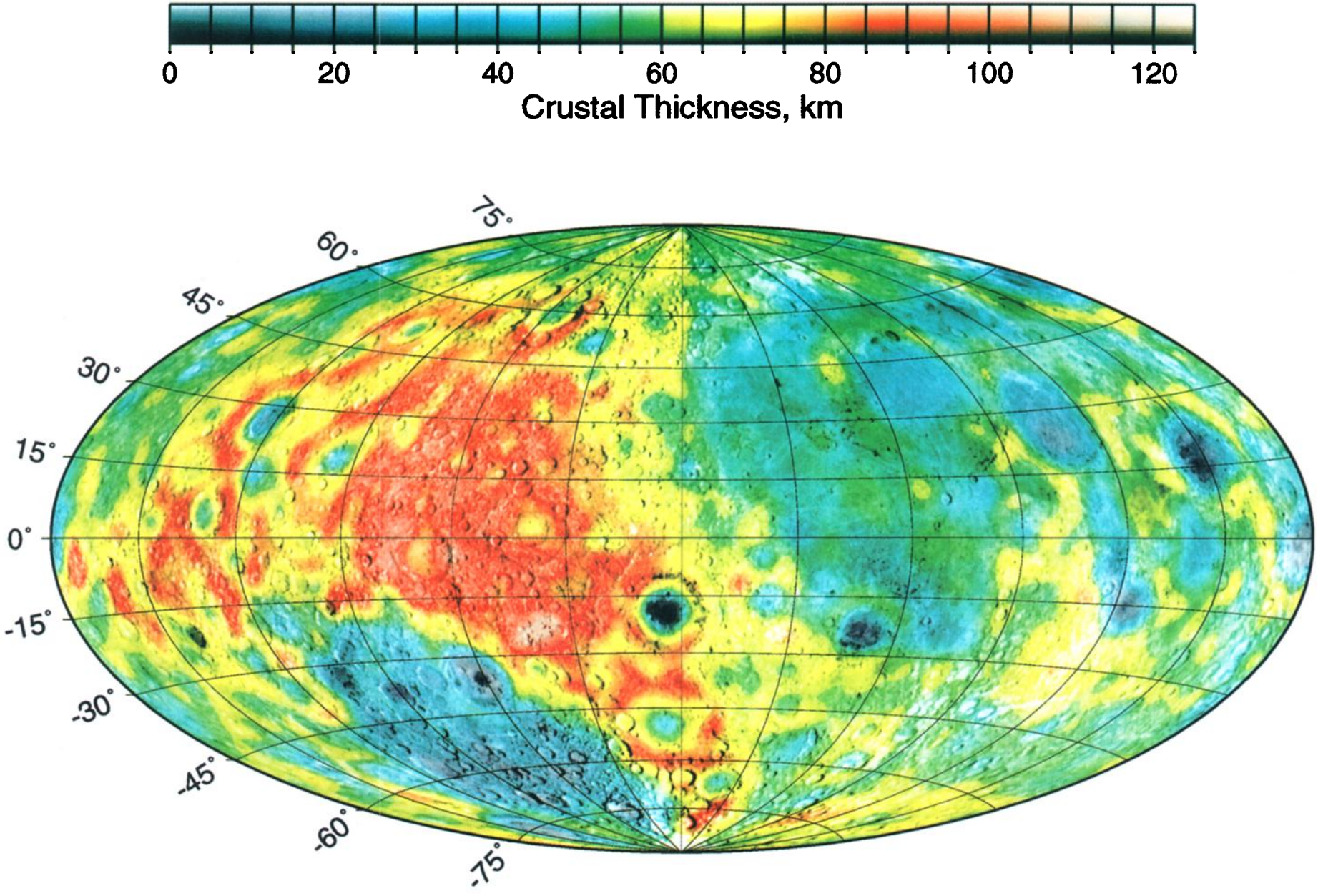

Plate 1. Plot of global crustal thickness showing major lunar basins sampled by Clementine. Hammer equal-area projection centered on 270°E, with nearside on the right; longitude gridlines at 30° intervals, latitude gridlines at 15° intervals. Corrections have been made for the gravitational attraction of mare fill in major impact basins. The remaining positive gravity anomalies are modeled by crustal thinning. On the farside (left), the South Pole-Aitken impact basin also shows unusually thin crust.

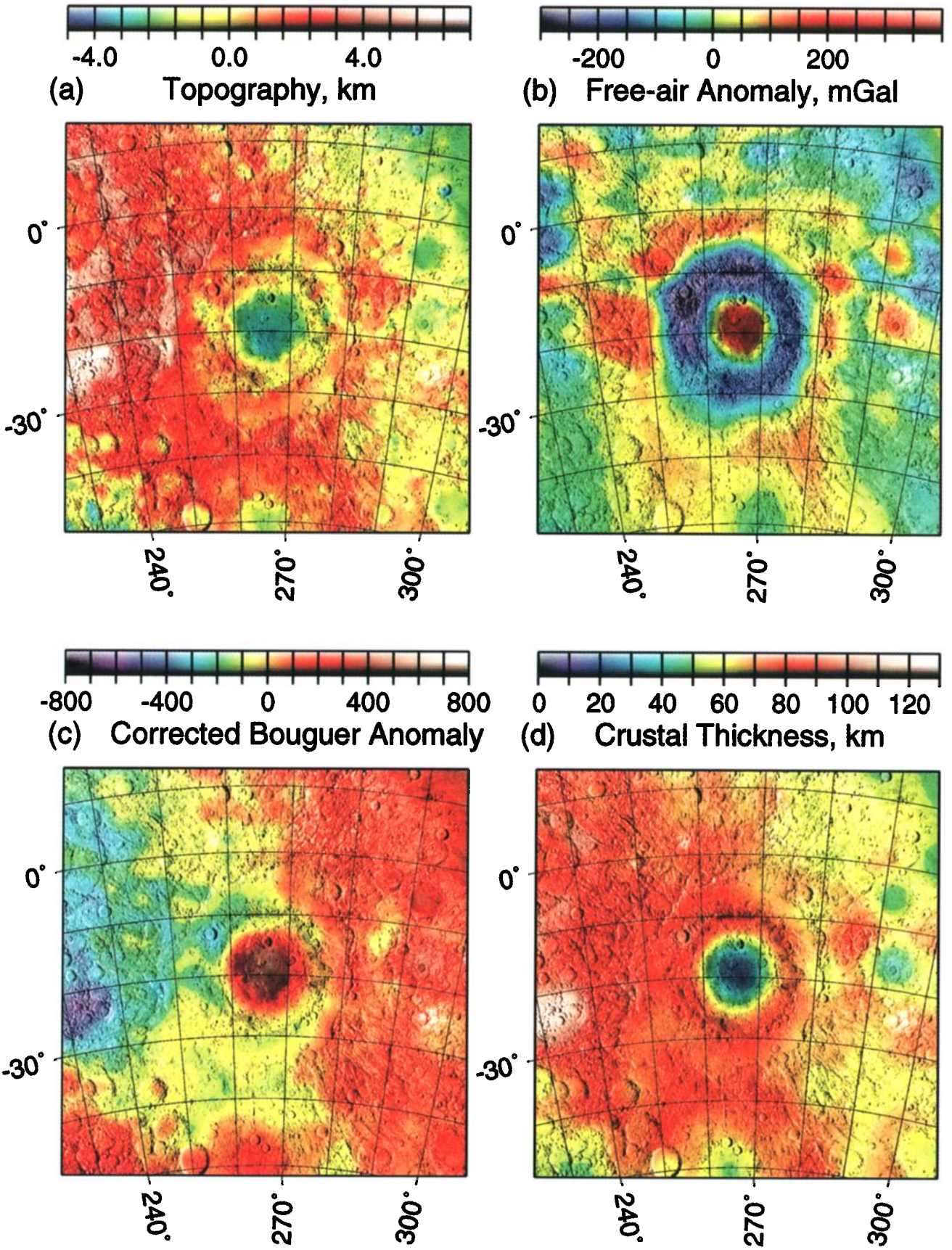

Plate 2. Oblique Mercator projected plots, approximately 2048 km square, showing regional inversion for Mare Orientale: (a) topography sampled from GLTM2, (b) gravity from lgm-0309b (c) complete Bouguer gravity anomaly corrected for a 1.7-km-thick, 300-km-diameter mare unit, and (d) crustal structure inferred from smooth downward continuation.

Table 1. Crustal Thickness of Lunar Basins (in Order of Decreasing Basin Diameter)

Longitude, deg	Latitude, deg	Radius, km	Basin	Thickness, km	Elevation, m
180.	-56.	1250.	SP-Aitken	33.0	-4710.
341.	36.	580.	Imbrium (342, 33)	36.3	-2740.
58.5	17.	530.	Crisium (58.5, 17.5)	20.3	-4100.
52.	-4.	495.	Fecunditatis	39.6.	-2130.
266.	-19.5	465.	Orientale (265, -20)	21.8	-3360.
94.5	-51.5	440.	Australe	57.9	-750.
34.	-16.	430.	Nectaris	24.7	-3330.
86.6	-2.4	420.	Smythii (87, -2)	26.3	-4250.
320.5	-24.	410.	Humorum	21.9	-2840.
40.	7.	400.	Tranquillitatis	54.5	-1460.
19.	26.	370.	Serenitatis (19, 27)	31.2	-3080.
297.5	40.	350.	NW Procellarum	47.8	-2650.
345.	-21.	345.	Nubium	46.4	-2910.
266.	-50.	315.	Mendel-Rydberg	51.1	-2200.
84.	58.	300.	Humboldtianum (86, 61)	34.8	-4610.
175.	18.5	300.	F-Sharonov	45.3	-3000.
232	2.5	285.	Hertzsprung(232,2)	71.7	320.
237.	52.	265.	C-Sarton	48.2	-2376.
147.	26.	220.	Moscoviense	39.8	-3840.
203.	-4.5	220.	Korolev	79.7	2120.
291.5	-5.5	215.	Grimaldi	42.9	-2450.
141.	6.	165.	Mendeleev	61.4	-1710.
340.	-3.	-	Apollo 12,14	55.0	-1830.

Locations in columns 1 and 2 are those used in this analysis. Locations in parentheses are those given by Wilhelms [1987]. All crustal thickness estimates have been corrected for mare fill where appropriate. Basin elevations are with respect to the reference spheroid discussed in D.E. Smith et al. (submitted manuscript, 1996)

to $\hat{\mathbf{g}}$ in the first term in equation (3). At large wavenumbers, this filter suppresses features that cannot be resolved in the presence of noise, while at small wavenumbers $w(\mathbf{k})$ approaches unity. The weights Λ_1 and Λ_2 specify the relative weights assigned to the squared norm of the slope and the curvature of the topography, respectively. Neglecting the higher order terms, this filter minimizes the slope and curvature of the topography. In addition, spatial sidelobes produced by abrupt truncation in the harmonic domain are avoided. Since the gravity is related in a nonlinear way to the topography, this minimization of slope and curvature is approximate. The second term in equation (3) is a correction for the 3-D effects of topography resulting from the first term. The correction term is smoothed and underrelaxed in order to damp out oscillations in the iteration. The iterations cease when they have converged to topography that generates the smoothed Bouguer anomaly, and the relative magnitude of the residual is less than 10^{-4}.

Figure 2 shows an example of the resolution of this filter. A cylindrical plug of mantle material (dashed lines) with a 125-km radius and 40-km thickness is used to generate a surface gravity map. A smoothing filter is applied with a corner (half-power) wavelength of 340 km. The smoothed gravity is then downward continued to the moho at 60-km depth. The first term in the expansion (2) overestimates the height of the cylinder (dotted curve), while the solution of (3) using terms up to n=4 provides a fairly close approximation (solid curve) to the actual moho profile. The finite-amplitude approach clearly stabilizes the inversion. The "ringing" or overshoot at the base by 1.7 km at a radius of 245 km is a slight artifact due to the sharp edge of the cylinder. Less than 200 m ringing results from inversions performed on the more gradual topography that results from geologic processes at the elevated temperatures of the early Moon.

The frequency response of the global and regional smoothing filters, and the resulting downward continuation factors, are shown in Figure 3. The global filter, with a corner wavelength of 480 km, is designed to attenuate the poorly constrained gravity over the farside, and its amplitude is less than 1% at spherical harmonic degree 70. The regional filter, at the 150-km minimum wavelength of the gravity field, attenuates the spectral response, but the downward continuation factor is nearly unity. Because we are minimizing the roughness of the resulting topography, our resolution decreases with increasing moho depth. On the lunar nearside, where average moho depth is 50-55 km, features of 150-km half wavelength are better resolved than in this example.

An example of the complete procedure is shown in Plate 2. Orientale, a 5-km-deep, 930-km-diameter basin on the edge of the farside highlands [*Head,* 1974], is the youngest of the major multiring impacts and exhibits the most extreme variation in gravity signal. The topography (Plate 2a) and gravity (Plate 2b) are gridded on a 2048-km-square region. The gravity is reduced using a surface density of 2800 kg m^{-3}, and corrected for a 1.7 km-thick, 300 km diameter mare to

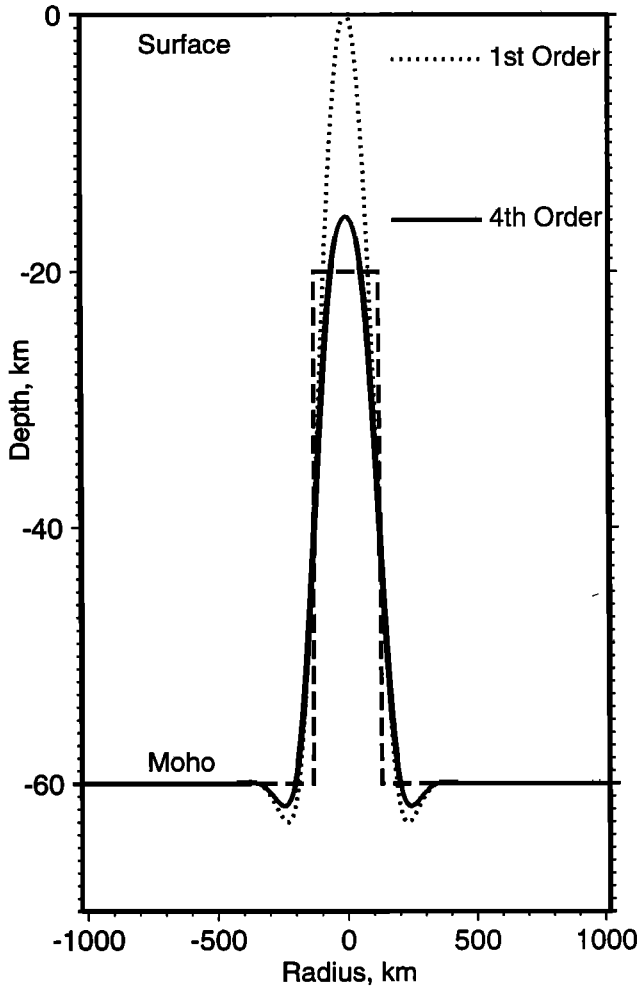

Figure 2. Cross section of a cylindrical mantle plug, and the geometry of the plug as determined by inversion of the gravity anomaly resulting from the plug. Dotted curve corresponds to the first-order, filtered downward continuation of the anomaly, while the solid curve is the result of the iterative solution of the inversion equation.

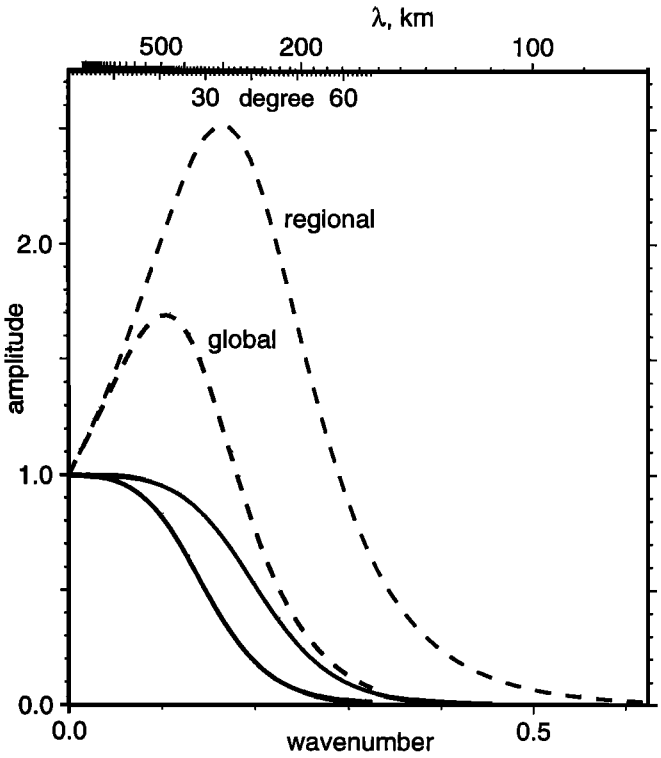

Figure 3. Frequency response of global and regional downward continuation filters. Dashed curves show the downward continuation factor applied at each degree or normalized wavenumber.

produce the CBA (Plate 2c). Downward continuation to an average depth of 69.7 km produces the crustal structure shown in (Plate 2d). The gravity anomaly of the crustal structure has an RMS residual of 30 mGal with respect to the observed anomaly, a residual variance of about 1% of the CBA signal, and about the same as the formal uncertainty in GLGM2 in this region.

The residual variance trades off with the magnitude of the Λ constraints. Equal weights for slope and curvature were assigned. The constraints adopted in this paper result in a trade-off between smoothness and data fit that, on the average, matches the errors in the gravity field. The RMS residual between filtered and observed CBA was between 13 and 43 mGal, depending on the region.

Results

Global Crustal Thickness

The mare-corrected Bouguer anomaly, when downward continued to a mass sheet 61 km below a nominal equatorial radius of 1738 km, matches a crustal thickness of 55 km near the Apollo 12 and 14 landing sites. Interpreting the mass sheet as variations in moho depth provides a first-order estimate of the variations in crustal thickness. This depth implies a crust composing 10% of the lunar volume. The mean depth to moho of 61 km is 13% less than was inferred by *Bills and Ferrari* [1977a]. The average thickness depends only slightly on the density contrast assumed (500 kg m^{-3}) between crust and mantle because the crustal thickness at the midpoint between the Apollo 12 and 14 sites is within 6 km of the lunar average.

The Moon has major spatial variations in crustal thickness (Plate 1), with a range of more than 100 km. The average thickness of the farside is 67 km, 12 km more than the nearside (55 km). The farside has greater variation in crustal thickness than the nearside (Figure 4). The nearside has a unimodal distribution, somewhat skewed by thin crust associated with mare basins, while the farside has an almost bimodal distribution, reflecting the thickened crust of the lunar highlands as well as the thin crust of the deep SP-Aitken basin.

The asymmetrical distribution of crust accounts for almost all of the offset of the center-of-figure of the Moon from its center-of-mass. In the spherical harmonic coefficients of topography of D. E. Smith et al. (submitted manuscript, 1996), this offset, first noted by *Kaula et al.* [1972], is 1.77 km away from the center of mass along the Earth-Moon axis. The total offset is 1.93 km in a direction 202° longitude and 7° latitude, toward thicker crust on the farside. Our results show that the center of crust is offset by 13.4 km from the center of mass toward 203° longitude and 8° latitude. The greater

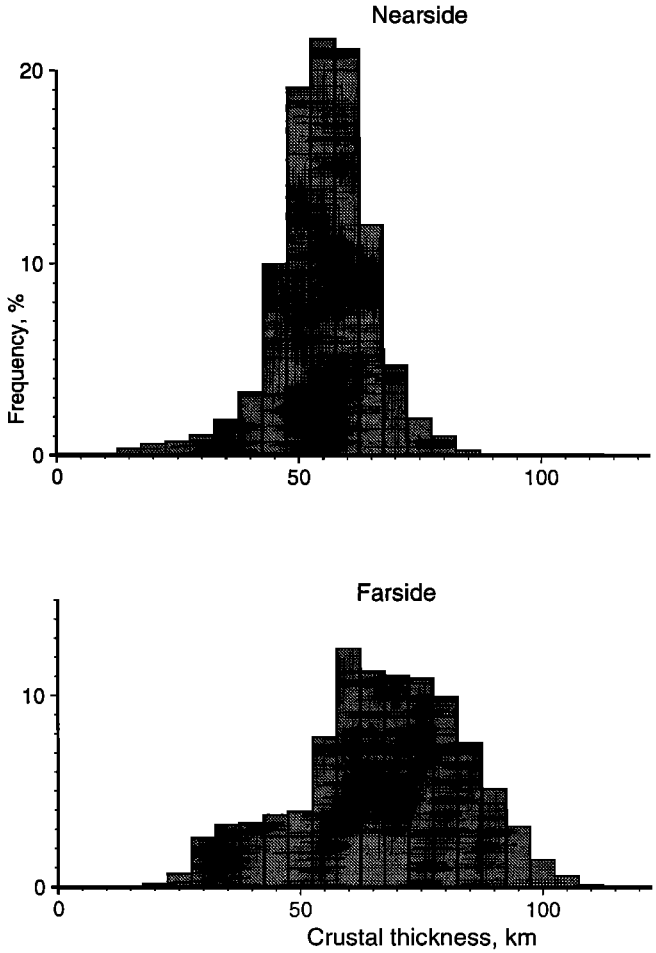

Figure 4. Histogram of crustal thickness of the lunar nearside and farside. Data were taken from an equal-area grid of global thicknesses, excluding the regions lacking data at the poles.

concentration of dense mare basalts on the nearside only accounts for about 3% of the center-of-figure offset.

The lunar crust is also preferentially distributed toward the equator. The degree 2 zonal coefficient of topography reveals more than 2-km flattening of the polar radius relative to the equator (D. E. Smith et al., submitted manuscript, 1996). This degree of flattening implies, on the average, a crust 9.5 km thicker at the equator than the poles. Most of this thickening is associated with the large area of thick crust on the farside north of the SP-Aitken basin, and a smaller component is due to the nearside southern highlands. The flattening of the geoid of 1/3234.93 determined by Lemoine et al. (submitted manuscript, 1995) may result mainly from the mass of the thickened crust at the equator.

Table 1 summarizes the crustal thickness at the centers of the major basins. The thickest crust (>120 km) lies south of Hertzsprung at (232°E, 22°S) while the thinnest (~20 km) appears to be associated with the centers of Crisium and Orientale. The extreme values are biased somewhat owing to the neglect of large-amplitude effects, but we may use average values over regions containing basins to constrain the average depth of moho in the corresponding regional inversions. All major nearside mare basins are thinned to 40 km or less: Imbrium, Crisium, Orientale, Nectaris, Smythii, Humorum, and Serenitatis. Some recognized mare basins without a clear ring structure, such as Australe, Nubium, and Tranquillitatis, have near-average thickness. Two farside basins, Humboldtianum and Moscoviense, are thinned to less than 40 km. The thinnest crust on the farside occurs beneath craters Apollo, Ingenii, Planck, Poincare, Schrodinger, and Zeeman, all within the preexisting SP-Aitken basin (Plate 1). This giant basin, nearly 1250 km in radius, represents the largest area of thin crust on the Moon, and is surrounded by thicker-than-average crust. Local thinning relative to the surroundings can also be resolved beneath highland basins such as Bailly, Coulomb-Sarton, Freundlich-Sharanov, Hertzsprung, Korolev, and Mendeleev, as well as many smaller basins.

Regional Maps

Regional inversions were applied to each of the major mascon basins: Imbrium, Crisium, Orientale, Nectaris, Smythii, Humorum, Serenitatis, and Grimaldi, as well as all other basins with diameters of 330 km or larger. Detailed maps of crustal thickness are shown in Figure 5. Except for SP-Aitken, each figure shows a 1600-km-across subset of the region used for inversion, relatively free of edge effects and distortion.

Orientale (Plate 2 and Figure 5), with 21-km-thick crust at the center, has the most extreme crustal thickness variations. Nearly 50 km of crust appears to have been excavated from its center, relative to a regional average of 70 km, to be replaced by upwarped mantle. Mendel-Rydberg (Figures 5b) shows less pronounced crustal thinning than nearby Orientale and Grimaldi. Both Grimaldi, the smallest of the mare mascons with a radius of 215 km, and Imbrium (the largest) exhibit much less thinning than Orientale. South of Grimaldi, the nonmare basin Cruger (293°E, 16°S), which was previously poorly resolved in lunar topography and gravity data, also has a mascon-like gravity anomaly and thin (30 km) crust.

Crustal structure appears to be azimuthally symmetric about each centrally thinned impact, although the symmetry is modified by surrounding basins. Figure 6 shows radial averages of basin and moho topography, using a running median filter to minimize the effects of surrounding perturbations. All the mascon basins show a similar pattern: a central uplifted mantle surrounded by a ring of thickened crust. The majority of this ring lies within the surface diameter of the crater. A possible secondary ring of uplifted mantle lies outside Orientale, Nectaris, and Smythii. Only in the case of Serenitatis does the bulk of the thickened ring extend well beyond the surface boundary. The margin of this basin is indistinct, overprinted with mare and Imbrian ejecta, and possibly extends 80 km further than the tabulated radius of 370 km.

Our inversion does not assume a compensation mechanism for basin structure, and suggests that the basin and moho topography are maintained by variable degrees of lithospheric stress. The dashed curves in Figure 6 show the surface profiles that would be required if the inferred moho relief were locally compensated by surficial topography, assuming a density of 2800 kg m^{-3}. Such a local isostatic model would not, however, match the observed gravity field. For example, over Orientale (Figure 6a), the youngest major basin, the surface topography mirrors the moho topography in an averaged sense, but the relief on the moho is not locally compensated

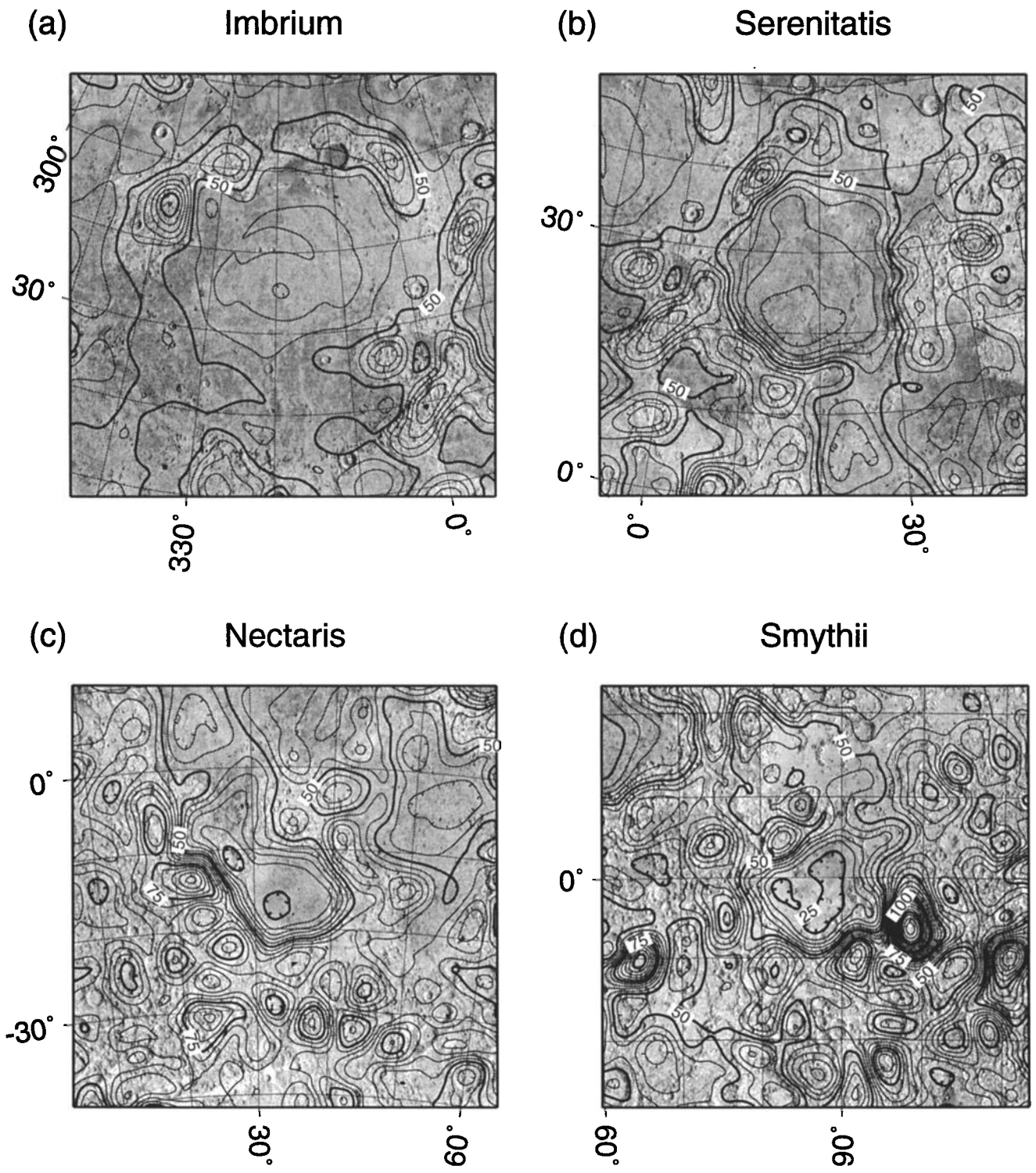

Figure 5. Detailed crustal thickness maps of major mare mascon basins. Contour interval 5 km, with major contours at 25 km. Regions are 1600 km square. (a) Imbrium, (b) Serenitatis, (c) Nectaris, (d) Smythii, (e) Crisium, (f) Humorum, (g) Grimaldi, (h) Orientale, (i) SP-Aitken.

by variations in crustal thickness. If near-isostatic adjustment had occurred, as argued by *Bratt et al.* [1985a,b], the present surface would represent the addition of nearly 4 km of crustal material at the center, after the lithosphere had developed sufficient strength to support an additional, superisostatic load [*e.g.*, *Wise and Yates,* 1970; *Solomon et al.,* 1982]. This is more than twice the amount of loading inferred by *Sjogren and Smith* [1977] and requires more mare flooding than we have assumed. At the same time, the depression of the moho surrounding the impact basins is not completely balanced by

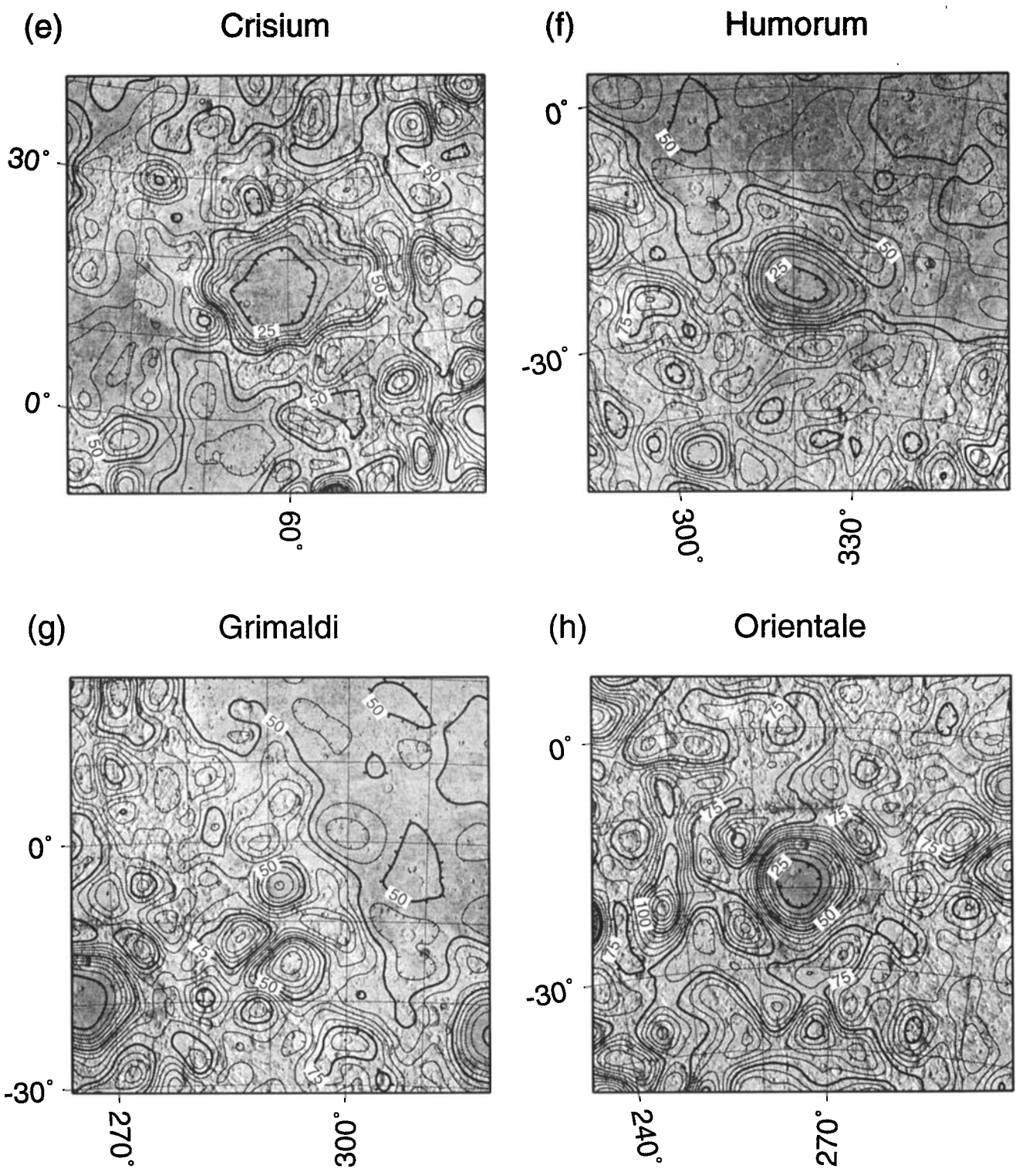

Figure 5. (continued)

rings of elevated crust. Such a situation does not occur with nonmare basins, such as Mendel-Rydberg (Figure 6b) or very large basins such as SP-Aitken (Figure 6c).

The crustal models in Figures 5 and 6 demonstrate that long-wavelength crustal thickness variations are mainly due to moho topography. Figure 7 summarizes the moho relief beneath major mare-filled and nonmare basins compared to the corresponding regional average depth to moho. A value of zero would indicate that the moho is undeformed, while positive values indicate that the moho beneath the basin is shallower than the surroundings and overlain by thinner crust. Crustal thinning beneath the basin is characteristic of both the mare and nonmare basins. Causes of this thinning are likely to be excavation of the basin cavity and mantle rebound

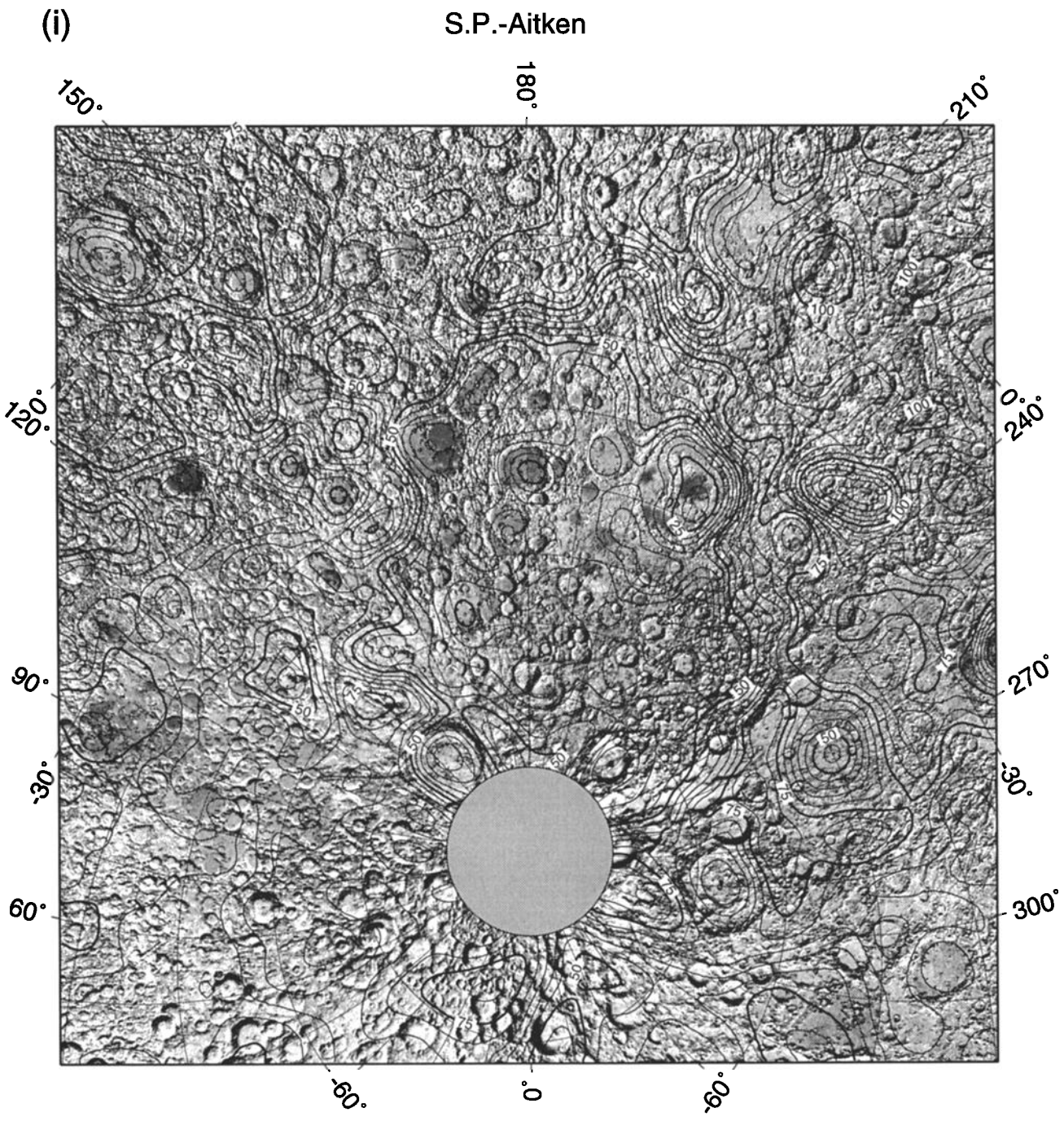

Figure 5. (continued)

associated with shock unloading in the impact process [*Melosh*, 1982; *Phillips and Dvorak*, 1982; *Bratt et al.*, 1985b]. The amount of mantle uplift does not correlate well with basin diameter (Figure 7a), as would be expected if the degree of rebound scaled with impact energy. There is a significant negative correlation between moho relief and age (Figure 7b), supporting the idea that older basins have partially recovered from their initial perturbed state. The correlation suggests that the younger, more fluid Moon was unable to fully maintain the uplift resulting from the impact process.

Giant Basins

The deepest basin, SP-Aitken, is more than twice as large as the next largest basin (Imbrium) and is significantly distorted by plane projection. We treat it separately, determining its crustal structure by global downward continuation. The highly asymmetric and degraded structure of SP-Aitken shows, on the average, thinned crust within a central 1000-km radius (Figure 6c), with thicker-than-average crust extending outward to nearly 1800 km. Impacts of later age have strongly modified the basin floor, obscuring the original structure. The crustal

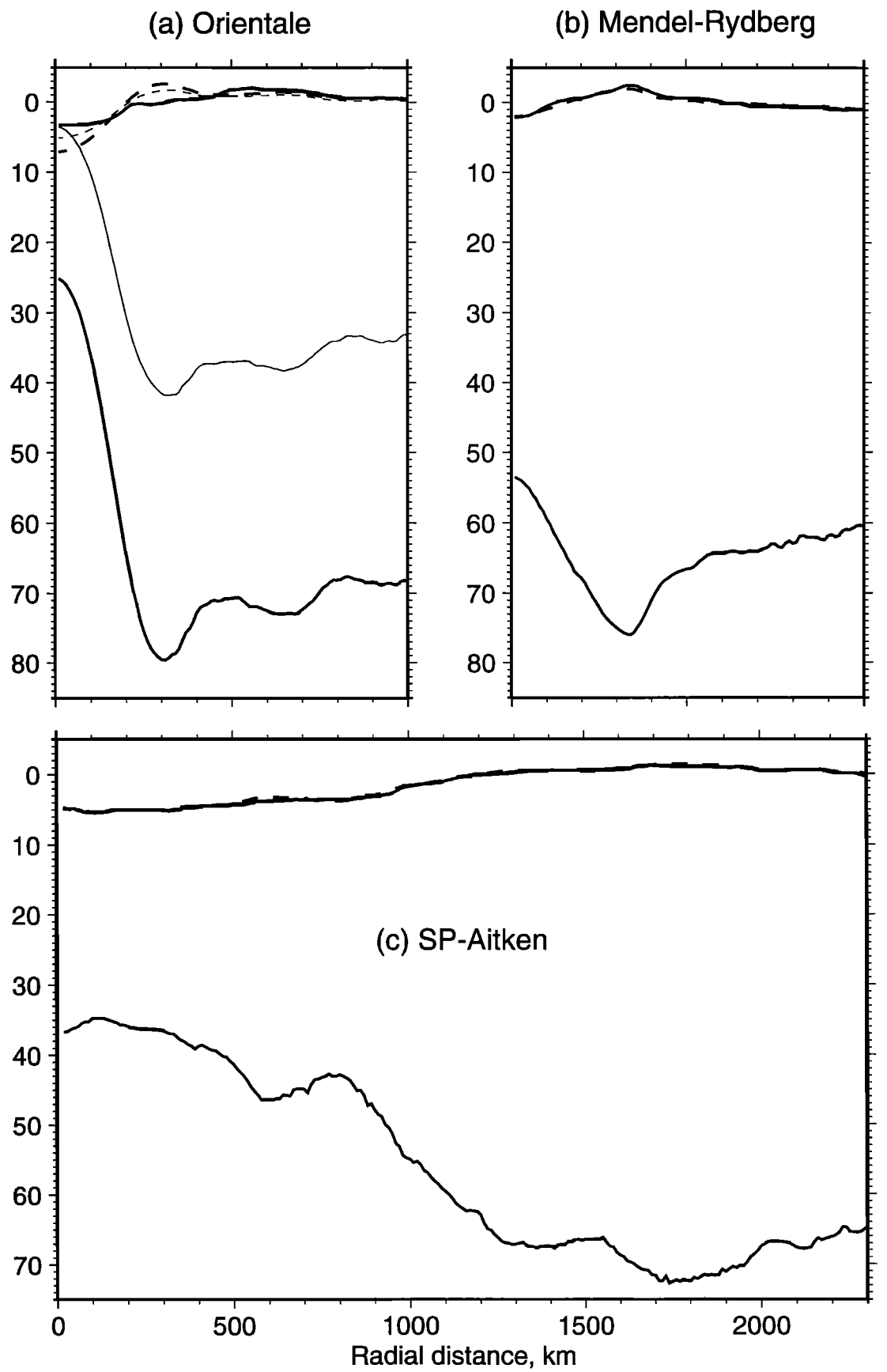

Figure 6. Radially averaged topography and moho of major mare basins. Vertical exaggeration 20:1. The dashed curves show the topography, with an arbitrary reference level, that would result if the inferred moho and surface topography were in local isostatic equilibrium. Most of the mare basins show deviations from local isostasy. (a) Orientale. A model with a moho reference level of 35 km (thin curves) would require uplift of moho to the surface, and also deviates from isostasy. (b) Mendel-Rydberg, (c) SP-Aitken, (d) Imbrium, (e) Crisium, (f) Nectaris, (g) Smythii, (h) Humorum, (i) Serenitatis, (j) Fecunditatis, (k) Grimaldi, (l) Australe, (m) Humboldtianum, (n) Tranquillitatis, (o) Nubium, (p) Korolev, (q) Hertzsprung, (r) Moscoviense, and (s) Mendeleev.

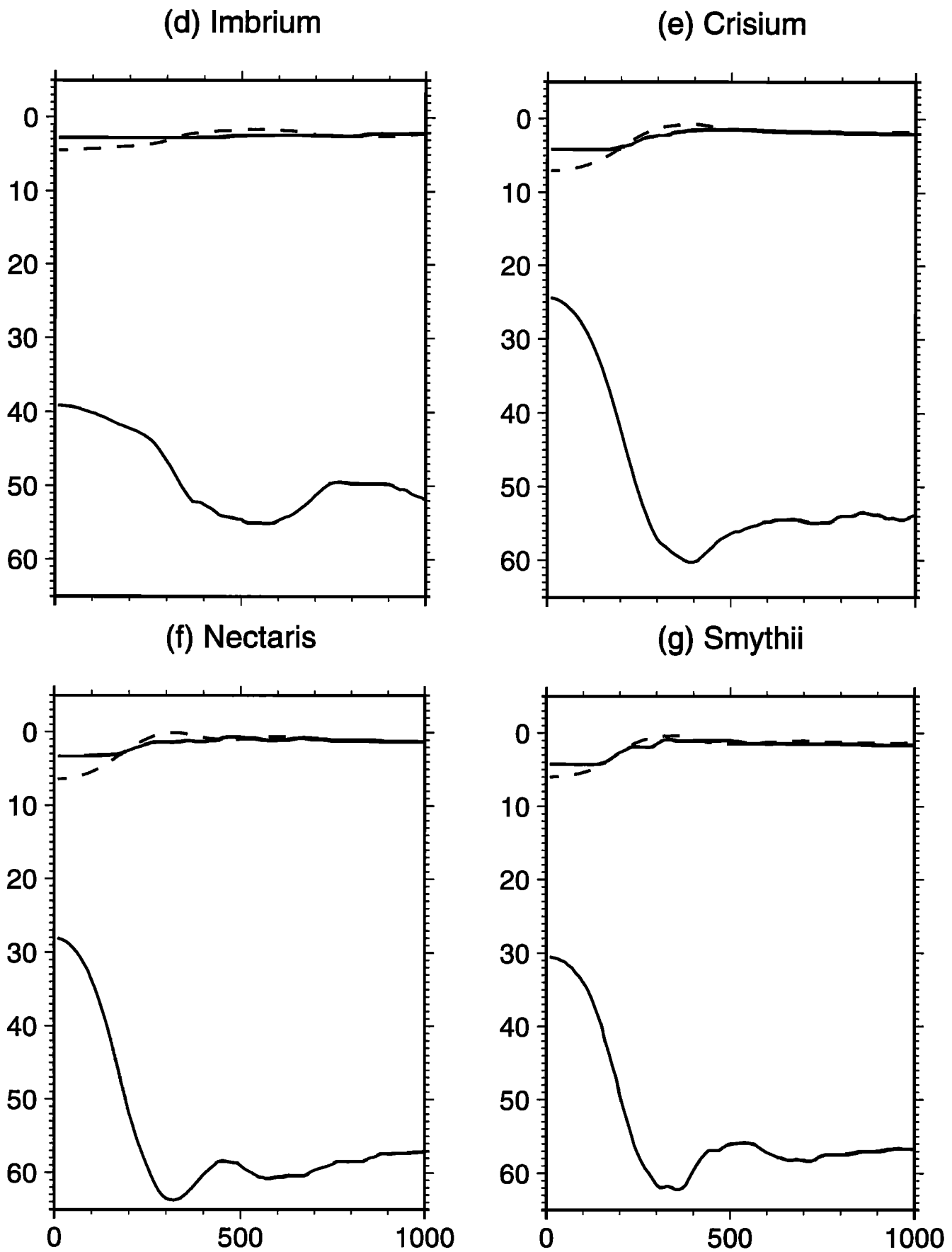

Figure 6. (continued)

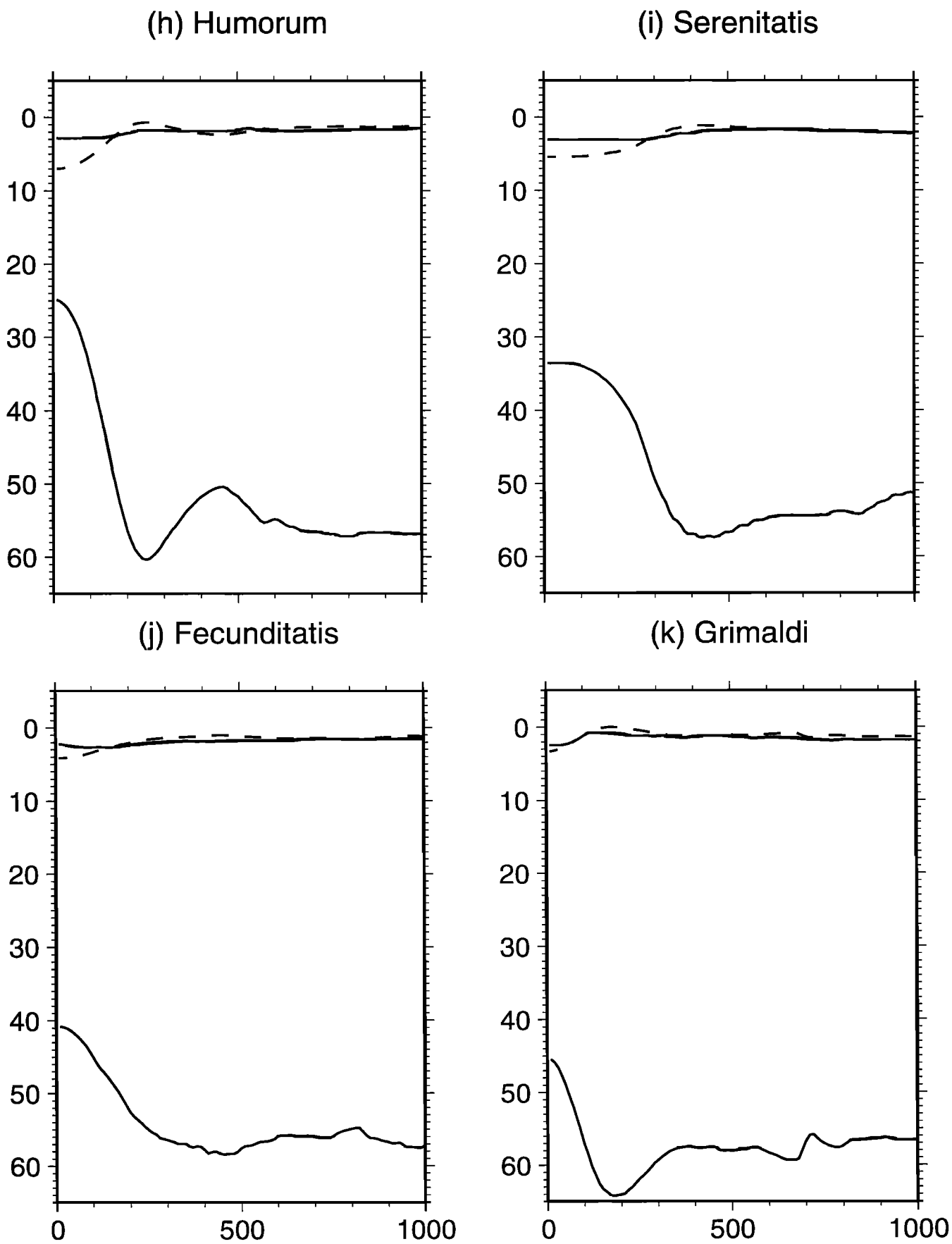

Figure 6. (continued)

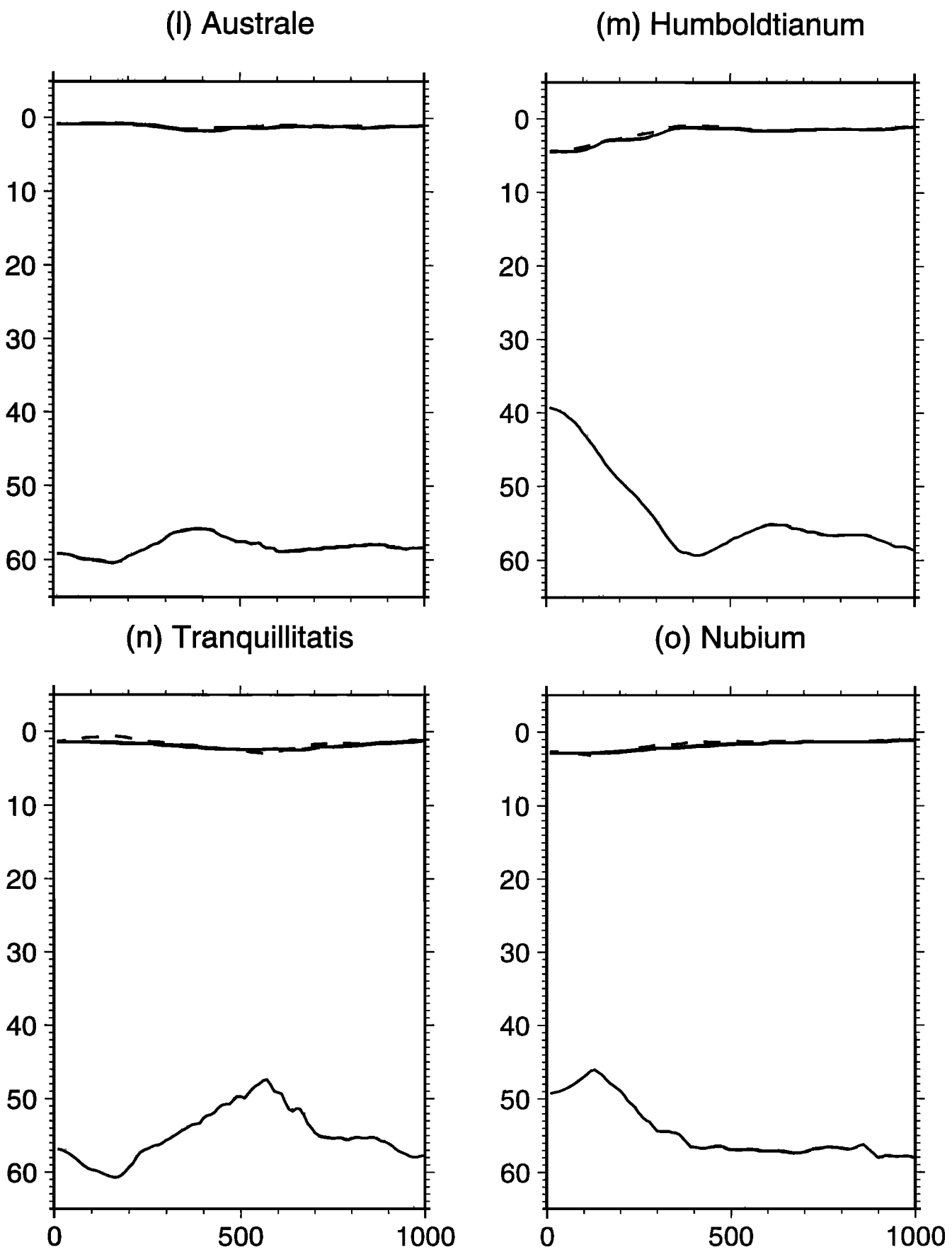

Figure 6. (continued)

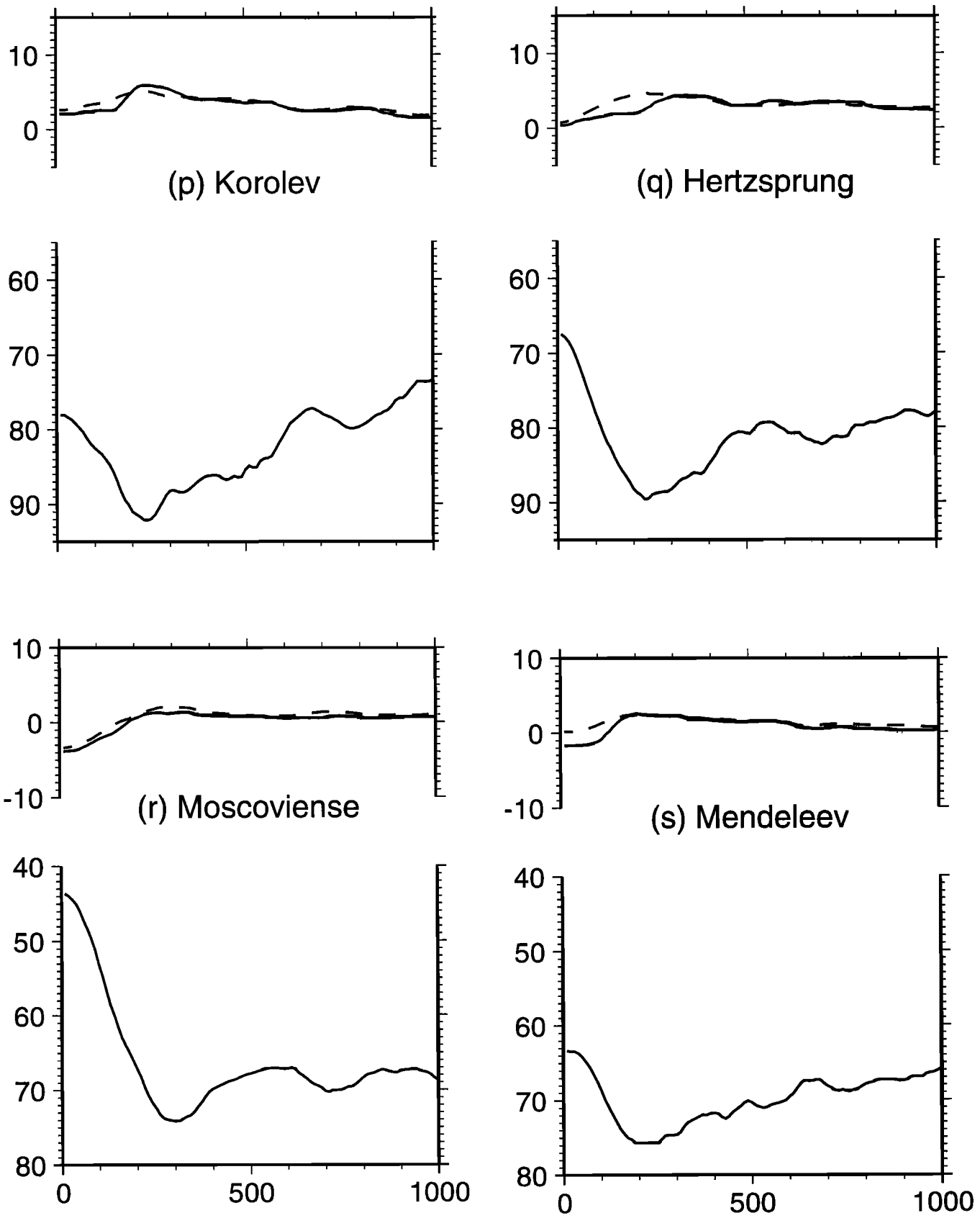

Figure 6. (continued)

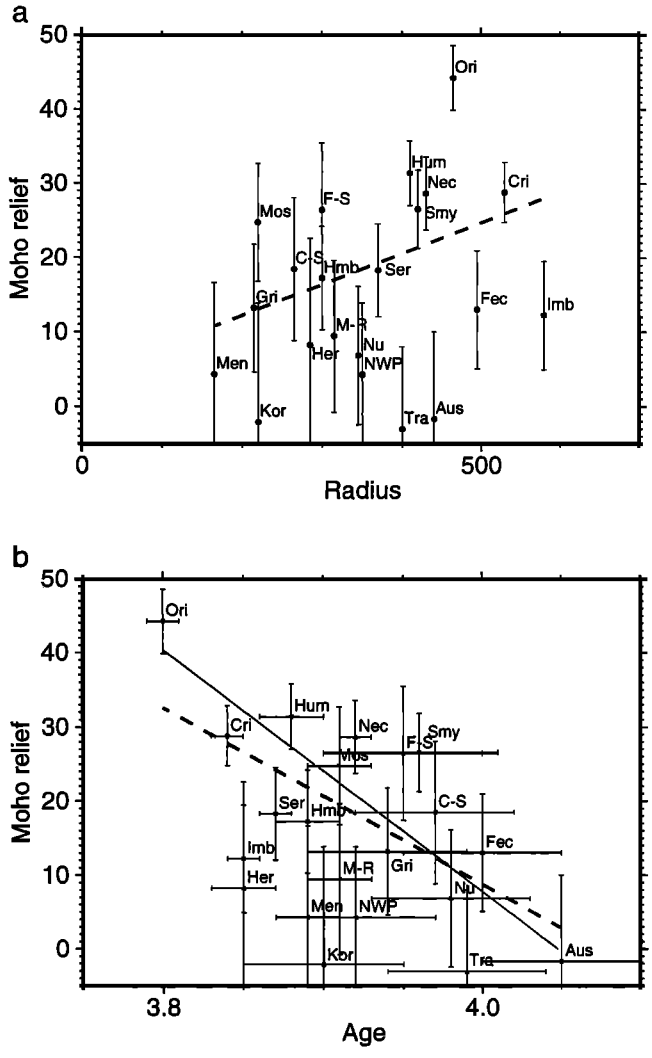

Figure 7. (a) Plot of central moho uplift relative to regional average versus basin size. Error bars reflect 20% uncertainty in density contrast at the moho. Weighted linear regression (dashed line) shows no significant correlation. (b) Plot of uplift versus basin age. Ages are from *Wilhelms* [1987] and references therein. Error bars for age are approximate, and are smallest for basins dated radiometrically from lunar samples. Linear regressions weighted for errors in uplift (dashed line) and jointly for errors in age and uplift (solid line) show decrease in relief with increasing age. Correlation is significant by Spearman rank test (α=0.05).

thickness of the basin is markedly thinner than the lunar average, and has remained so since its formation more than 4.1 Gyr ago.

One of the most striking features of this basin is the arc of elevated topography and thickened crust that surrounds it to the northeast (Plate 1). We have questioned the origin of the extremely thick crust of the highlands to the north [*Zuber et al.*, 1994], and suggested that it could be a consequence of regional, large-scale melting and/or possibly at least in part due to the effects of basin-forming impact. Given its proximity to the SP-Aitken basin we speculate that this pattern of crust could be associated with oblique impact by a large, massive projectile. Assuming a normal incidence at a velocity of 20 km s^{-1}, a meteoroid of at least 215-km diameter would be required to produce a transient cavity of 2250-km diameter, according to a simple scaling law [*Melosh*, 1989, equation 7.8.1c]. An oblique impact would result in lower cratering efficiency and require a proportionately larger projectile. If the vertical component of velocity were as low as the lunar escape velocity, 2.4 km s^{-1}, its diameter would be about 900 km. The pattern of ejecta seen in laboratory-scale oblique impacts is asymmetric [*Melosh*, 1989], with a stronger downrange component, but whether these experimental results can be extrapolated to such a large scale is a matter of debate. Excavation of the original crust with asymmetric distribution of ejecta could certainly contribute to the unevenly distributed crust of the lunar farside (Figure 4).

Zuber et al. [1994] noted from its muted gravity signature that SP-Aitken is nearly fully compensated. While a radially averaged plot (Figure 6c) shows a near equilibrium between surface topography and moho relief, individual basins within it, such as Apollo, exhibit negative free-air anomalies. The crustal structure of SP-Aitken appears to be overprinted by these later impacts, occuring after most of the primary structure had undergone viscous relaxation. A rough calculation indicates that the impact could have raised crustal temperatures by 500°C, reducing its strength [*Bratt et al.*, 1985b].

A giant (3200-km diameter) pre-Nectarian basin in Oceanus Procellarum was postulated [*Whitaker*, 1981; *Wilhelms*, 1987] on the basis of the arcuate highland terrain surrounding the front-side mare. Based on Clementine topography and the global crustal thickness, this feature would be centered at approximately 345°E, 22°N. *McEwen and Shoemaker* [1995] claimed that diameter/depth relationships derived from Clementine altimetry support the existence of the Procellarum basin. However, radially averaged profiles about this axis show about 10 km of moho relief within a 2000-km radius (Figure 8), but do not show a distinct central high and surrounding trough. The scatter of surface and moho topography about the running median suggests much overprinting by known basins and provides no definite evidence of the proposed giant impact. Much of the thinning can be ascribed to the Imbrium impact and other nearside basins. The giant basin, had it existed, must have been highly asymmetrical or predated the formation of the thick crust and elevated topography of the highlands south of Serenitatis and Nectaris. A large impact could have contributed dramatically to the global asymmetry of crust, but the fact that the center-of-crust to center-of-mass offset lies in a direction about 40° from the axis of the basin suggests that this could not be the sole reason for the asymmetry. Other explanations, such as differentiation due to large-scale internal convection [*Lingenfelter and Schubert*, 1973] must be considered. The crustal asymmetry is not significantly greater than would result from random processes with a power spectrum similar to other planets [*Bills and Kobrick*, 1985], but correlates with composition [*Lucey et al.*, 1995].

McEwen et al. [1994] proposed on the basis of historical data that a large topographic low in the northwestern mare represents a roughly 700-km diameter basin at 297.5°E, 42°N. We have included the NW Procellarum basin in our study, as the topography from Clementine confirms the topographic low [*Zuber et al.*, 1994], and we find a local minimum in crustal thickness (47 km) near the center. However, the gravity anomaly is negative near the center, and the crustal thickness variations are diffuse (Figure 6m).

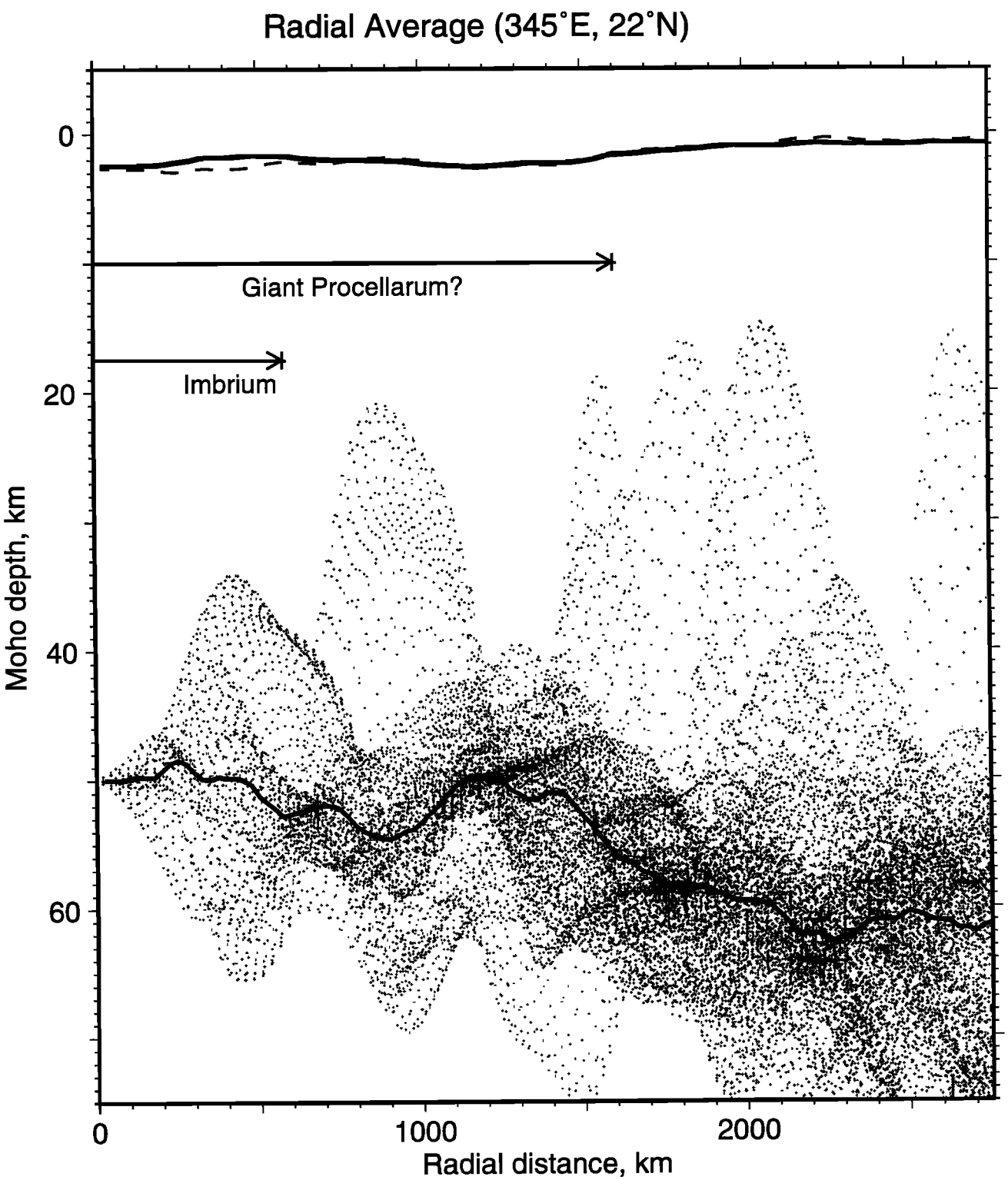

Figure 8. Radially averaged moho and surface topography of the proposed 1600-km-radius, giant Procellarum basin, at 40:1 vertical exaggeration. Medians shown by solid curves. Individual points illustrate scatter about the median. Imbrium (341°E, 36°N) radius shown for comparison.

Discussion

The crustal structure as revealed by Clementine represents a significant advance over the Apollo era knowledge [*Bratt et al.*, 1985a], in its coverage of high-latitude regions and improved long-wavelength resolution of the farside. The addition of near-global topography makes it possible to derive crustal thickness over major basins in a consistent fashion, assuming moderate corrections for mare basalt. The

large dynamic range of global crustal thickness requires major spatial variations in melting of the lunar exterior and/or significant impact-related redistribution of lunar crust [*Zuber et al.*, 1994].

The Clementine crustal models presented here are in general agreement with those obtained by the spatio-spectral localization technique of *Solomon and Simons* [1996] for the lunar highlands, but differ from those of *Wieczorek and Phillips* [1996], who attempt to resolve vertical stratification in crustal density. A mascon model of *Kiefer and Dodge* [1996] matches the gravity high at the center of Orientale basin by means of a 3- to 4-km-thick layer of uncompensated basalt emplaced over an Airy-compensated basin and moho model. Such a model requires substantially greater mare emplacement than has been estimated previously, and cannot simply account for the ring of negative gravity anomaly surrounding the mascon.

The simplified, end-member case of lunar density stratification in which a uniform density crust and mantle is assumed provides one possible interpretation of the observed Bouguer gravitational signatures of lunar basins. At each step of the analysis, we have been cautious in our assumptions in order to minimize the possible excursions from a uniformly stratified Moon. In this context, the basin structures that we have delineated are likely to be more pronounced, especially at shorter wavelengths than can presently be resolved.

The accuracy of the crustal models presented is limited mainly by the uncertainty of gravity data [cf. *Zuber et al.*, 1994], particularly from the lunar farside, and uncertainty in the lateral heterogeneity of crustal density. There are significant density variations due to changes in composition [e.g., *Thurber and Solomon*, 1978]. The lower density of the anorthositic highlands could partially compensate their elevated topography, but the 1.7-km difference in average elevation between nearside and farside (D. E. Smith et al., submitted manuscript, 1996) requires nearly 3% difference in average crustal density, which is larger than that inferred from compositional mapping by *Solomon* [1978]. Another factor that we have not considered is possible lateral variations in mantle density [*Wasson and Warren*, 1980; *Finnerty et al.*, 1988]. For a mantle which has undergone a major amount of melt extraction, say 20%, the density change will be comparable to that due to a 200°-300°C temperature change (E.M. Parmentier, personal communication, 1995). If the pressure is high enough (i.e., depth is great enough) that garnet is one of the minerals melted, the effect could be as high as 500°C. The corresponding density changes for these cases compared to the density of an unmelted mantle are 0.9% and 1.5%, which corresponds to at most two milligals of gravity per extra kilometer of depleted mantle. While it is possible that the hot interior, through internal dynamic processes, could support the stresses needed to maintain such large heterogeneities following the cessation of melting, further study of this process is required.

All of the impact basins studied show a consistent pattern of thinned crust toward the center, and thickened crust near the rim. Crustal thinning is consistent with magnesium-rich exposures in central peaks [*Pieters*, 1982] and other compositional anomalies associated with large basins [*Belton et al.*, 1994]. The composition of the basin materials is generally more mafic [*Belton et al.*, 1994; *Lucey et al.*, 1995] than the surrounding highlands, and is thought to represent samples of the lower crust. Crustal excavation is a natural consequence of the impact process, but the thickened crust surrounding the basins suggests that much of this crust is deposited as ejecta or is displaced laterally at depth.

The clear pattern of mass excess under the mascons, indicated by gravity highs, and the ring of mass deficit around them, indicated by gravity lows, is robust under any reasonable assumptions. As discussed in more detail by Lemoine et al. (submitted manuscript, 1995), the pattern we describe was first seen in line-of-sight tracking accelerations [*Muller and Sjogren*, 1968, 1972; *Sjogren et al.*, 1973; *Muller et al.*, 1974], and thus is not a consequence of "ringing" induced in the spherical harmonic gravity modeling procedures. In the case of Orientale, the central mass excess and lack of isostatic equilibrium does not depend on the constraints used to obtain the gravity solutions.

The underlying excess masses evident in Bouguer gravity (i.e., Plate 2) are present in all of the basins, even those lacking a visible free-air-gravity high. Nor are the "mascons" unique to mare basins, as shown by Mendel-Rydberg (Figure 6b), Hertzsprung (Figure 6q), and Korolev (Figure 6p). The gravity signature of the mantle plugs is simply obscured in areas of thicker crust by their greater depth.

It is possible that we have overestimated the depth of the density interface producing the central highs, or that the gravity anomaly results from a shallow transition to denser crust, with further deflections in the lower crust. We tested this by ascribing all of the Bouguer gravity to a single shallow interface. If the "moho" under Orientale were at an average depth of 35 km instead of the 70 km we estimated from our global model (Figure 6a, thin curves), the moho would rise to the surface beneath the basin center. The amplitude of this model would be somewhat less than our preferred model, but the topography and deeper interface would still be out of equilibrium.

We see in Figure 6 that some of the present-day topography over basins is maintained by stresses in the lithosphere. While large impacts may produce sufficient heat to weaken the lithosphere and lead to subsequent relaxation [*Solomon et al.*, 1982], our data support the suggestion of *Taylor* [1982] that the mascons are principally due to rapid mantle uplift (formed immediately as a consequence of the impact and not due to a long-term isostatic response), followed by an additional component of mare basalt filling.

Within individual basins, it is possible that impact-related brecciation and comminution of ejecta with crust creates a ring of lower-density material [e.g., *von Frese et al.*, 1996] that is partially responsible for gravity moats around the mascons. It is difficult to envision a mechanism whereby magma would flood the mare without intruding and welding the more porous surrounding material. Moreover, crustal density models derived from Apollo seismic data [*Toksoz et al.*, 1972] suggest that the gravity moats, which are many tens of milligals less than the regional average, cannot be explained solely by brecciation.

Another possibility is that some of the ring of thickened crust and depression of moho could be due to flexure of the lithosphere under surface (mare flooding) and subsurface (crustal thinning) loading. A reasonable model would have to explain both the broad scale of the gravity lows and their substantial magnitude, within reasonable ranges of elastic parameters. Models of this type can only partially explain the rings of thickened crust [*Williams et al.*, 1995]. Further investigation of the possible flexural origin of the ringing thickened crust is under way by K. K. Williams et al. (manuscript in preparation, 1996).

While analysis of lithospheric stress and lunar density variations continues, we are confident that most of the variation between and within basins is due to crustal structure. We note that thickening of crust outside the central region of crustal thinning of the basin has not been identified in association with well-studied, but smaller, terrestrial impact basins [*Pilkington and Grieve,* 1992]. It is natural to question whether differences in the thermal, mechanical, or compositional structure of the lithosphere can explain this fundamental difference in basin structure. Another possibility is that the impact process itself is responsible for a ringed structure involving the lunar mantle, producing crustal thinning at the center of the basin in conjunction with crustal thickening at the edge. Possible evidence for this hypothesis comes from the juxtaposition of the highest topography and thickest crust along the north rim of SP-Aitken, with the deepest topography and thin crust within the basin. All but the oldest basins show similar patterns of moho topography, with central highs and surrounding moats, neither of which is compensated by surface topography. A dynamic mechanism for their formation is required. One possible mechanism would be the brief period of acoustic fluidization [*Melosh,* 1979; *Melosh and Gaffney,* 1983] following the impact event, enabling large-scale deformation by pressure waves resulting from impact to be frozen in place, via the Bingham fluid rheology of *Melosh* [1989]. In this scenario, subsequent modification via faulting during collapse of the transient crater cavity [cf. *Croft,* 1981; *Melosh,* 1989, 1995] and ductile flow [*Solomon et al.,* 1982] would be insufficient to erase the frozen-in potential energy created by the impact process except possibly in the case of the oldest basins such as SP-Aitken. Significant future modeling efforts will be required to quantitatively test these hypotheses and better understand the mechanism of crustal thickening that characterizes major lunar basins.

Conclusions

New gravity and topography from the Clementine mission have enabled analysis of the global- and regional-scale nature of the lunar crust. The global map, which includes corrections for the gravitational attraction of basaltic fill in mare basins, indicates that both mare and nonmare basins exhibit thinning of the crust beneath the basin. The large range of global crustal thickness implies major spatial variations in melting of the lunar exterior and/or significant impact-related redistribution of lunar crust. This observation, in combination with evidence for variable isostatic compensation states of lunar basins [*Zuber et al.,* 1994], dictates that a much better understanding of the relationship of major impacts and crustal formation will be required in order to understand the Moon's early thermal structure.

Downward continuation and filtering of the complete Bouguer anomaly has revealed detailed crustal structure for the major lunar mascon basins. Basin structure is characterized by a central region of thinned crust with a conjugate ring of thickened crust lying mainly within the basin rim. The observed pattern indicates a deep structural component to lunar basin rings which has not been identified in terrestrial impact basins. Surface topography associated with major basins is not fully compensated by the variations in crustal thickness. This observation provides additional evidence that the lunar lithosphere in the vicinity of basins had achieved significant rigidity around the time of basin formation [*Zuber et al.,* 1994]. These results hold the promise of providing constraints on the relative importance of the impact process and subsequent isostatic adjustment in forming the characteristic, surficial multiring structure.

Acknowledgments. We thank Pedro Rustan and the members of the Clementine team for the success of the mission, and acknowledge the assistance of Anita Brenner, Dave Rowlands, Sue Fricke, and Greg Elman in reducing the data. We express appreciation to Jason Phipps Morgan and Donna Blackman for sharing their downward continuation program, and to Kevin Williams for extensive discussions and finding several mistakes We thank Jay Melosh for reviewing the manuscript; in addition, we acknowledge an informal 3-hour-long oral review of the paper by Sean Solomon. The GMT software of *Wessel and Smith* [1991] was used extensively in the analysis. This work was supported by grants to M.T.Z. from the NASA Planetary Geology and Geophysics Program and NASA Lunar and Asteroid Data Analysis Program.

References

Baldwin, R. B., The tsunami model of the origin of ring structures concentric with large lunar craters, *Phys. Earth Planet. Inter., 6,* 327-339, 1972.

Belton, M. J. S. et al., Galileo multispectral imaging of the north polar and eastern limb regions of the Moon, *Science, 264,* 1112-1115, 1994.

Bills, B. G., and A. J. Ferrari, A harmonic analysis of lunar topography, *Icarus, 31,* 244-259, 1977a.

Bills, B. G., and A. J. Ferrari, A lunar density model consistent with topographic, gravitational, librational, and seismic data, *J. Geophys. Res., 82,* 1306-1314, 1977b.

Bills, B. G., and A. J. Ferrari, A harmonic analysis of lunar gravity, *J. Geophys Res., 85,* 1013-1025, 1980.

Bills, B G , and M. Kobrick, Venus topography: A harmonic analysis, *J. Geophys. Res., 90,* 827-836, 1985.

Bowin, C , B. Simon, and W R. Wollenhaupt, Mascons: A two-body solution, *J. Geophys. Res., 80,* 4947-4955, 1975.

Bratt, S. R., S. C. Solomon, J. W. Head, and C. H. Thurber, The deep structure of lunar basins: Implications for basin formation and modification, *J. Geophys. Res., 90,* 3049-3064, 1985a

Bratt, S. R., S. C. Solomon, and J. W. Head, The evolution of impact basins: Cooling, subsidence, and thermal stress, *J. Geophys. Res., 90,* 12,415-12,433, 1985b.

Conel, J. E., and G. B. Holstrom, Lunar mascons: A near-surface interpretation, *Science, 162,* 1403-1405, 1968.

Constable, S. C., R. L. Parker, and C. G. Constable, Occam's inversion: A practical algorithm for generating smooth models from EM sounding data, *Geophysics, 52,* 289-300, 1987.

Croft, S. K., The modification stage of basin formation: Conditions of ring formation, in Multi-ring Basins, edited by P. H. Schultz and R. B. Merrill, *Proc. Lunar Planet. Sci. Conf., 12A,* 227-257, 1981.

Davies, M. E., T. R. Colvin, and D. L. Meyer, A unified lunar control network: The near side, *J. Geophys. Res., 92,* 14,177-14,184, 1987.

DeHon, R. A., Thickness of mare material in the Tranquillitatis and Nectaris basins, *Proc. Lunar Sci. Conf., 5th,* 53-59, 1974.

DeHon, R. A., Mare Humorum and Mare Nubium: Basalt thickness and basin-forming history, *Proc. Lunar Sci. Conf., 8th,* 633-641, 1977.

DeHon, R. A., Maximum thickness of materials in the western mare basins (abstract), *Proc. Lunar Planet. Sci. Conf., 9th,* 229-231, 1978.

DeHon, R. A., Thickness of western mare basalts, *Proc. Lunar Planet. Sci. Conf., 10th,* 2935-2955, 1979.

DeHon, R. A., and J. D. Waskom, Geologic structure of the eastern mare basins, *Proc. Lunar Planet. Sci. Conf., 7th,* 2729-2746, 1976.

Dence, M. R., Dimensional analysis of impact structures (abstract), *Meteoritics, 8,* 343-344, 1973.

Finnerty, A. A., R. J. Phillips, and W. B. Banerdt, Igneous processes and closed system evolution of the Tharsis region of Mars, *J. Geophys. Res., 93,* 10,225-10,235, 1988.

Franklin, J. N , Well-posed stochastic extensions of ill-posed linear problems, *J. Math. Anal. Appl., 31,* 682-716, 1970.

Goins, N. R., A. M. Dainty, and M. N. Toksoz, Lunar seismology: The internal structure of the Moon, *J. Geophys. Res., 86,* 5061-5074, 1981.

Hartmann, W. K., and G. P. Kuiper, Concentric structures surrounding lunar basins, *Commun. Lunar Planet. Lab., 1,* 51-66, 1962.

Head, J. W., Orientale multi-ringed basin interior and implications for the petrogenesis of lunar highland samples, *Moon, 11,* 327-356, 1974.

Head, J. W., Lava flooding of ancient planetary crusts: Geometry, thickness, and volumes of flooded lunar impact basins, *Moon Planets, 26,* 61-88, 1982.

Horz, F., How thick are lunar mare basalts?, *Proc. Lunar Planet. Sci. Conf., 9th,* 3311-3331, 1978.

Kaula, W.M., *Theory of Satellite Geodesy (Applications of Satellites to Geodesy),* 124 pp., Blaisdell, Waltham, Mass., 1966.

Kaula, W. M., G. Schubert, R. E. Lingenfelter, W. L. Sjogren, and W. R. Wollenhaupt, Analysis and interpretation of lunar laser altimetry, *Proc. Lunar Sci. Conf., 3rd,* 2189-2204, 1972.

Kaula, W. M., G. Schubert, R. E. Lingenfelter, W. L. Sjogren, and W. R. Wollenhaupt, Lunar topography from Apollo 15 and 16 laser altimetry, *Proc. Lunar Sci. Conf., 4th,* 2811-2819, 1973.

Kaula, W. M., G. Schubert, R. E. Lingenfelter, W. L. Sjogren, and W. R. Wollenhaupt, Apollo laser altimetry and inferences as to lunar surface structure, *Proc. Lunar Planet. Sci. Conf., 5,* 3049-3058, 1974.

Kiefer, W.S., and M.C. Dodge,Uncompensated mare basalts as a model for lunar mascons, *Lunar Planet. Sci. Conf., XXVII,* 665-666, 1996.

Konopliv, A. S., W. L. Sjogren, R. N. Wimberly, R. A. Cook, and V. Alwar, A high resolution lunar gravity field and predicted orbit behavior, paper presented at the AIAA Astrodynamics Specialist Conference, Am. Inst. of Aeronaut. and Astronaut., Victoria, B.C., Canada, 1993.

Lingenfelter, R. E., and G. Schubert, Evidence for planetary convection from first order topography, *Moon, 7,* 172-180, 1973.

Lucey, P.G., G.J. Taylor, and E. Malaret, Abundance and distribution of iron on the Moon, *Science, 268,* 1150-1153, 1995.

McEwen, A.S., and E.M. Shoemaker, Two classes of impact basins on the Moon (abstract), *Lunar Planet. Sci. Conf., XXVI,* 935-936, 1995.

McEwen, A., P. Davis, A. Howington-Kraus, and M. Davies, Evidence for a pre-Nectarian impact basin in northwestern Oceanus Procellarum (abstract), *Lunar Planet. Sci. Conf., XXV,* 869-870, 1994.

Melosh, H. J., Acoustic fluidization: A new geologic process?, *J. Geophys. Res., 84* , 7513-7520, 1979.

Melosh, H. J., A simple mechanical model of Valhalla Basin, Callisto, *J. Geophys. Res., 87,* 1880-1890, 1982.

Melosh, H. J., *Impact Cratering: A Geologic Process*, 245pp., Oxford University Press, New York, 1989.

Melosh, H. J., Under the ringed basins, *Nature, 373,* 104-105, 1995.

Melosh, H. J. and E. S. Gaffney, Acoustic fluidization and the scale dependence of impact crater morphology, *Proc. Lunar Sci. Conf. 13th,* Part 2, *J. Geophys. Res., 88,* suppl., A830-A834, 1983.

Morrison, L. V., and R. J. Martin, A digitized version of C. B. Watts' charts of the marginal zone of the Moon, *Moon, 2,* 463-467, 1971.

Muller, P. M., and W. L. Sjogren, Mascons: Lunar mass concentrations, *Science, 161,* 680-684, 1968.

Muller, P. M. and W. L. Sjogren, Rings, in *The Moon, IAU Symp. 47,* edited by S.K Runcorn and H.C. Urey, 35 pp., 1972.

Muller, P., W. L. Sjogren, and W. R. Wollenhaupt, Lunar gravity: Apollo 15 Doppler radio tracking, *Moon, 10,* IAU Symp. 47, 195-205, 1974.

Müller, R. D., and W. H. F. Smith, Deformation of the oceanic crust between the North American and South American plates, *J. Geophys. Res., 98,* 8275-8291, 1993.

Nakamura, Y., G. V. Latham, H. J. Dorman, A.-B. K. Ibrahim, J. Koyama, and P. Horvath, Shallow moonquakes: Depth, distribution and implications as to the present state of the lunar interior, *Proc. Lunar Planet. Sci. Conf., 10th,* 2299-2309, 1979.

Nozette, S., et al., The Clementine mission to the Moon: Scientific overview, *Science, 266,* 1835-1839, 1994.

Oldenburg, D. W., The inversion and interpretation of gravity anomalies, *Geophysics, 39,* 526-536, 1974.

Parker, R. L., The rapid calculation of potential anomalies, *Geophys. J. R. Astron. Soc., 31,* 447-455, 1972.

Parker, R. L., and S. P. Huestis, The inversion of magnetic anomalies in the presence of topography, *J. Geophys. Res., 79,* 1587-1593, 1974.

Phillips, R. J. and J. Dvorak, The origin of lunar mascon basins: Analysis of the Bouguer gravity associated with Grimaldi, in Multi-ring Basins, edited by P. H. Schultz and R. B. Merrill, *Proc. Lunar Planet. Sci. Conf., 12,* 91-104, 1981.

Phillips, R. J., J. E. Conel, E. A. Abbot, W. L. Sjogren, and J. B. Morton, Mascons: Progress toward a unique solution for mass distribution, *J. Geophys. Res., 77,* 7106-7114, 1972.

Phipps Morgan, J., and D. K. Blackman, Inversion of combined gravity and bathymetry data for crustal structure: A prescription for downward continuation, *Earth Planet. Sci. Lett., 119,* 167-179, 1993.

Pieters, C. M., Copernicus crater central peak: Lunar mountain of unique composition, *Science, 215,* 59-61, 1982.

Pilkington, M., and R. A. F. Grieve, The geophysical signature of terrestrial impact craters, *Rev. Geophys., 30,* 161-181, 1992.

Scott, D. H., The geologic significance of some lunar gravity anomalies, *Proc. Lunar Sci. Conf., 5th,* 3025-3036, 1974.

Sjogren, W. L., and J. C. Smith, Quantitative mass distribution models for Mare Orientale, *Proc. Lunar Planet. Sci. Conf., 7th,* 2639-2648, 1976.

Sjogren, W. L., R. N. Wimberly, and W. R. Wollenhaupt, Lunar gravity via the Apollo 15 and 16 subsatellites, *Moon, 9,* 115-128, 1973.

Smith, W. H. F., and P. Wessel, Gridding with continuous curvature splines in tension, *Geophysics, 55,* 293-305, 1990.

Solomon, S. C., Mare volcanism and lunar crustal structure, *Proc. Lunar Sci. Conf., 6th,* 1021-1042, 1975.

Solomon, S. C., The nature of isostasy on the Moon: How big a Pratt-fall for Airy models?, *Proc. Lunar Planet. Sci. Conf., 9th,* 3499-3511, 1978.

Solomon, S. C., and J. W. Head, Lunar mascon basins: Lava filling, tectonics and evolution of the lithosphere, *Rev. Geophys., 18,* 107-141, 1980.

Solomon, S.C., and M. Simons, The isostatic state of the lunar highlands form spatio-spectral localization of global gravity, topography, and surface chemistry (abstract), *Lunar Planet. Sci. Conf., XXVII,* 1245-1246, 1996.

Solomon, S. C., R. P. Comer and J. W. Head, The evolution of impact basins: Viscous relaxation of topographic relief, *J.Geophys. Res., 87,* 3975-3992, 1982.

Spudis, P. D., *The Geology of Multi-Ring Impact Basins: The Moon and Other Planets,* Cambridge University Press, New York, 1993.

Spudis, P. D., R. A. Riesse, and J. G. Gillis, Ancient multiring basins on the Moon revealed by Clementine laser altimetry, *Science, 266,* 1848-1851, 1994.

Talwani, M., G. Thompson, B. Dent, H. Kahle, and S. Buck, Traverse gravimeter experiment, Apollo 17 Preliminary Science Reports, *NASA Spec. Publ., SP-330,* 13-1:13-13, 1973.

Taylor, S.R., *Planetary Science: A Lunar Perspective,* Lunar Planet. Inst., Houston, Texas, 1982.

Thurber, C. H., and S. C. Solomon, An assessment of crustal thickness variations on the lunar near side: Models, uncertainties, and implications for crustal differentiation, *Proc. Lunar Planet. Sci. Conf., 9th,* 3481-3497, 1978.

Toksoz, M. N., F. Press, A. Dainty, K. Anderson, G. Latham, M. Ewing, J. Dorman, D. Lammlein, G. Sutton, and F. Dunnebier, Structure, composition, and properties of the lunar crust, *Proc. Lunar Sci. Conf. 3, Geochim. Cosmochim. Acta Supp.,* 2527-2544, 1972.

Van Dorn, W. G., Tsunamis on the Moon, *Nature, 220,* 1102-1107, 1968.

von Frese, R.R.B., L. Tan, L.V. Potts, C.J. Merry, and J.D. Bossler, Lunar crustal modeling of Mare Orientale from Clementine satellite observations (abstract), *Lunar Planet. Sci. Conf., XXVII,* 1363-1364, 1996.

Wasson, J. T., and P. H. Warren, Contribution of the mantle to the lunar asymmetry, *Icarus, 44,* 752-771, 1980.

Watts, C. B., The marginal zone of the Moon, *Astron. Pap. Washington XVII,* U.S. Nautical Almanac Office, Washington, D.C., 1963.

Wessel, P., and W. H. F. Smith, Free software helps map and display data, *Eos Trans. AGU, 72,* 441, 443-445, 1991.

Whitaker, E. A., The lunar Procellarum basin, in Multi-ring Basins, *Proc. Lunar Planet. Sci. Conf. 12,* part A, 105-111, 1981.

Wieczorek, M.A., and R. J. Phillips, The structure and compensation of the lunar highland crust (abstract), *Lunar Planet. Sci. Conf., XXVII,* 1431-1432, 1996.

Wilhelms, D.E., The Geologic History of the Moon, *U.S. Geol. Surv. Prof. Pap., 1348,* 302 pp., U.S. Gov't. Printing Office, Washington, D.C., 1987.

Williams, K.K., G. A. Neumann, and M. T. Zuber, Lunar mascon basins: Analysis of effective elastic thickness using gravity anomaly

models (abstract), *Lunar Planet. Sci. Conf., XXVI,* 1505-1506, 1995.
Williams, K.K., and M.T. Zuber, Revised mare thicknesses (abstract), *Lunar Planet. Sci. Conf., XXVII,* 1441-1442, 1996.
Wise, D. U. and M. Y. Yates, Mascons as surface relief on a lunar "Moho," *J. Geophys. Res., 75,* 261-268, 1970.
Wong, L., G. Buechler, W. Downs, W. Sjogren, P Muller and P Gottlieb, A surface layer representation of the lunar gravity field, *J Geophys. Res., 76,* 6220-6236, 1971.
Wong, L., W. Downs, W. Sjogren, and P. Muller, A lunar mass distribution from Apollo 14, 15, and 16 CDM-LM and subsatellite radio Doppler data, Jet Propul. Lab., Pasadena, Calif., 1975.
Wood, J. A., Bombardment as a cause of the lunar asymmetry, *Moon, 8,* 73-103, 1973.
Zuber, M. T., D. E. Smith, F. G. Lemoine and G. A. Neumann, The shape and internal structure of the Moon from the Clementine mission, *Science, 266,* 1839-1843, 1994.

G.A. Neumann, Department of Earth and Planetary Sciences, Johns Hopkins University, Baltimore, MD 21218. (e-mail: Gregory.Neumann@jhu.edu)

D.E. Smith, F.G. Lemoine, Laboratory for Terrestrial Physics, NASA Goddard Space Flight Center, Greenbelt, MD 20771.

M.T. Zuber, Department of Earth, Atmospheric and Planetary Sciences, 54-518, Massachusetts Institute of Technology, Cambridge, MA 02139.

(Received August 21, 1995; revised March 27, 1996; accepted April 2, 1996.)